BUESCHKE, NIKOLAUS. M.S. Transforming a neural circuit to function without oxygen or glucose delivery: Balancing energy supply and demand in the brain. (2022)
Directed by Dr. Joseph Santin. 50 pp.

Inadequate delivery of oxygen and glucose to the brain leads to disruption in circuit function and behavior that ultimately results in irreversible excitotoxicity and neuronal death. Due to the prominence of these energetic insults in ischemic strokes, drug overdoses, cardiac arrest, and other medical cases, there is an increasing interest in how to overcome these significant energetic stressors on the brain. One such method of insight has been to observe adaptations in vertebrate species that have evolved to survive low-oxygen environments. Although many hypoxia tolerant species have been identified and thoroughly studied, hypoxia tolerance is largely “hard-wired” in these species. Here, we demonstrate an animal, the American bullfrog (*Lithobates catesbeianus*), that is capable of massively improving its ability to survive during hypoxia and ischemia upon emergence from aquatic overwintering. Cold-acclimation induces prolonged fictive respiratory motor output in hypoxia and ischemia, where function until energetic failure shows a >20-fold improvement from warm-acclimated controls**.** Because network activity continues despite the apparent loss of energy delivery, we have sought to determine the different types of plasticity that occur during aquatic overwintering from both energetic and physiological standpoints to improve tolerance to energetic stress. Through a series of pharmacological experiments, we determined that energy was primarily supplied by anaerobic glycolysis, fueled in tandem by localized brain glycogen stores. In addition, the main Ca^{2+} permeable glutamate receptor involved in synaptic transmission, NMDA receptors, decreased Ca^{2+} permeability and increased desensitization in neurons following aquatic overwintering. These results suggest that energetic demands are being decreased for costly neuronal processes to compensate for reduced ATP yield. In sum, the metabolic plasticity we observe may serve as a roadmap to improve tolerance of the brain to energetic stress in other species thought to be intolerant of hypoxia.

TRANSFORMING A NEURAL CIRCUIT TO FUNCTION WITHOUT OXYGEN AND GLUCOSE DELIVERY: BALANCING ENERGY SUPPLY AND DEMAND IN THE BRAIN

by

Nikolaus Bueschke

A Thesis

Submitted to

the Faculty of The Graduate School at

The University of North Carolina at Greensboro

in Partial Fulfillment

of the Requirements for the Degree

Master of Science

Greensboro

2022

Approved by

Dr. Joseph Santin
Committee Chair

APPROVAL PAGE

This thesis written by Nikolaus Bueschke has been approved by the following committee of the Faculty of The Graduate School at The University of North Carolina at Greensboro.

Committee Chair

Dr. Joseph Santin

Committee Members

Dr. Louis-Marie Bobay

Dr. Paul Steimle

July 7, 2022

Date of Acceptance by Committee

July 7, 2022

Date of Final Oral Examination

ACKNOWLEDGEMENTS

I would like to acknowledge my advisor, Dr. Joseph Santin, for going above and beyond to ensure my professional growth within these short two years. His enthusiasm and wealth of knowledge in physiology combined with his patience as a mentor have driven my interest in pursuing my Ph.D. in the field. I would also like to thank my committee members, Dr. Louis-Marie Bobay and Dr. Paul Steimle for their support and guidance in crafting this research from an experimental and communicative perspective.

I would also like to extend my gratitude to colleagues in the Santin Lab, specifically, Dr. Lara do Amaral Silva, Min Hu, and Sasha Adams for their contribution to this research. In addition, everybody in the lab has collectively instilled a welcoming environment into the workspace. Because of their benevolence, sense of humor, and support that they all have shown, I genuinely felt at home in the lab throughout my time there.

TABLE OF CONTENTS

LIST OF FIGURES

CHAPTER I: INTRODUCTION

Neurons require a substantial amount of energy to properly function within a circuit. If this fails to occur, brain function and behavior collapses. Most of these costs are seen in synaptic vesicle cycling, action potential propagation, and maintaining ion concentrations in response to ongoing activity (Bordone et al., 2019). Irreversible brain damage occurs following an event that results in inadequate neuronal energy supply generally observed in an ischemic stroke, drug overdose, heart attack, sleep apnea, and others. All of these energetic insufficiencies result from inadequate oxygen and/or glucose supply, leading to the massive release of glutamate and “excitotoxic” cell death within minutes in severe hypoxia (Ferdinand & Roffe, 2016). Current treatment strategies aimed at preventing cellular damage in energetic stress is largely centered around acclimating tissue to low oxygen to temporarily increase hypoxic tolerance. Despite showing some success, this treatment strategy effectively requires the knowledge of the exact date and time a stroke will occur and is therefore unreliable as a treatment (Li et al., 2017). One useful way to gain insights into overcoming brain dysfunction during energy stress has been to study the evolutionary adaptations of animals that can survive hypoxia (Larson et al., 2014). This thesis provides insight into the mechanisms of a neural circuit that has been recently identified to transform towards an energetically stress-tolerant state.

In vertebrates, aerobic metabolism generates most of the neuron’s ATP, whereas the absence of oxygen would lead to insufficient ATP production to fuel neural circuit activity. There have been several vertebrate species discovered to yield a higher tolerance to diminished oxygen than most other vertebrates, and are consequentially given the term, “hypoxia-tolerant”. These species can be categorized into two primary strategies that are used to overcome this metabolic stress that we can define as the “inhibitory” and the “persistent” strategies. The inhibitory strategy involves a dramatic reduction of overall brain activity during a hypoxic event

to conserve limited energy and is largely seen in species that undergo extended torpor such as the arctic ground squirrel and freshwater turtle (Frerichs et al., 1994; Pamenter et al., 2011). This strategy is thought to be achieved by the activation of neuronal energy sensors that detect indicators of falling ATP levels (hypoxia itself, decrease in ATP/ADP ratio, increased AMP, *etc.*), leading to an adaptive shutdown of neuronal function aimed toward preventing depletion of ATP. The persistent strategy allows for continuous neural activity during brain energy stress, which is necessary for species that are commonly exposed to such conditions when active. This strategy has been demonstrated in hooded seals and crucian carp (Bickler & Buck, 2007; Czech-Damal et al., 2014). Mechanisms that are thought to contribute to this strategy have been shown to include upregulation in brain glycogen stores (Kerem et al., 1973), as well as reduced metabolic rate through decreases in body temperature.

The American Bullfrog, *Lithobates catesbeianus*, is not typically viewed as a hypoxia tolerant species. However, our lab recently identified a brain circuit in this species that can transition to function for >20-fold longer during anoxia and ischemic stress than when in control conditions. This is the greatest functional improvement documented in any vertebrate (Bueschke et al., 2021). This network usually stops after 5-10 minutes during oxygen deprivation (Figure 1A, anoxia onset at blue box). This response is similar to what is observed in mammals experiencing metabolic failure; a large depolarization event followed by no activity during anoxia (Somjen, 2001). Remarkably, after animals come out from a simulated hibernation environment this same circuit produces activity for 3-4 hours during hypoxia. Another important aspect of this network is that it is a complicated circuit that operates by the most costly form of synaptic transmission (glutamate receptor-dependent synaptic transmission) to produce a behaviorally-relevant output. Therefore, this system allows us to study mechanisms that cause a circuit to switch between hypoxia-intolerant and tolerant states (warm-acclimated, WA; cold-acclimated, CA; respectively) with direct relevance to motor behavior, which is critical for the health of humans during a brain energy crisis.

Figure 1. Transformation of the respiratory circuit to hypoxia-resistant state. (A) Respiratory motor output is disrupted after less than 10 minutes in severe hypoxia. (B) Respiratory output persists with normal activity for up to 4 hours in severe hypoxia.

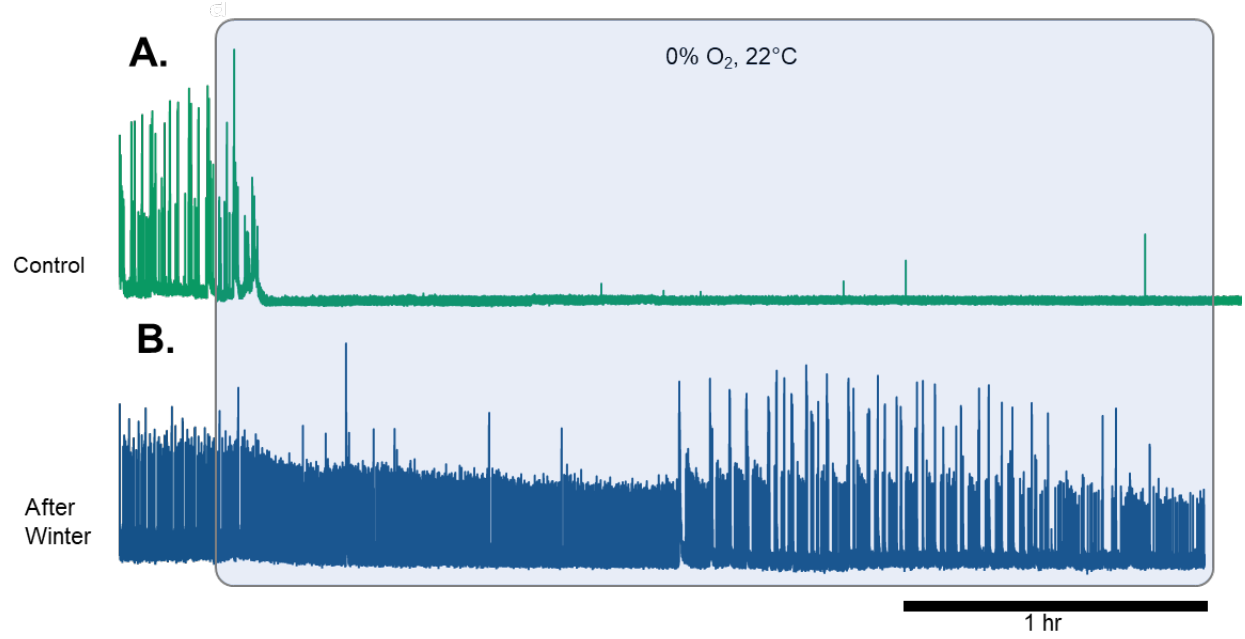

What physiological changes allow this network to become so remarkably resistant to anoxic stress? Given that we observed a dramatic improvement in neuronal function without aerobic metabolism, anaerobic processes are likely to contribute to ATP production. However, glycolysis only yields approximately 1/15 of the ATP than what is produced through aerobic metabolism per glucose molecule. Thus, the hypoxia-tolerant network in the American bullfrog needs to conserve this limited energy for neuronal survival in hypoxia while also somehow maintaining functional output. These results suggest that switching to a hypoxia-tolerant state also involves improving the efficiency of costly physiological processes, such as synaptic function and action potential firing. This question can be addressed by determining changes in energetic supply and demand. In terms of supply, there must be a shift in primary energy supplying mechanisms since aerobic mechanisms (TCA cycle and electron transport chain) are halted in the absence of oxygen. Alternative energetic supply mechanisms would likely result in a net decrease in available energy compared to a normal system and would potentially require a network-wide boost in efficiency to reduce energy demand. Therefore, the premise of this thesis

is that the network boosts its energy supply (chapter 4), while simultaneously reducing its energetic demands (chapter 5) to maintain homeostasis during hypoxia and ischemia.

CHAPTER II: AIMS

Specific Aim 1: Determine the degree to which glycolytic processes support circuit function during anoxia.

In severe hypoxic conditions, aerobic processes that produce ATP are stopped. Although the TCA cycle and electron transport chain is effectively inhibited in the absence of oxygen, glycolysis can persist. While the theoretical ATP yield is significantly reduced in these conditions, purely glycolytic pathways have been shown to adequately fuel respiratory motor networks in *L. catesbeianus* tadpoles (Winmill et al., 2005). In addition, glycogen stores within the brain are increased in winter frogs (McDougal et al., 1968), suggesting that endogenous substrates for glucose metabolism could support neuronal function after hibernation. Thus, I hypothesize that the CA bullfrog is capable of switching to primarily glycolytic metabolism to overcome anoxic stress which is fueled in tandem with glycogen localized in the brain. To test this, I observed the effect of various metabolic enzyme blockers in the presence of severe hypoxia on the *in vitro* frog brainstem to isolate the metabolic processes that occur.

Primary Expected Results

With effective glycolytic block on the hypoxia tolerant brainstem, I expect to see metabolic failure on a timescale that is more similar to the control than the unperturbed hypoxia tolerant brain when exposed to hypoxia. Despite glycolysis yielding less than 10% of ATP compared to O_2-dependent metabolic yields, alternative fuel sources have yet to be observed in vertebrates that can supply activity for a prolonged time. Thus, glycolysis seems like the most likely candidate. However, exogenous glucose supply should be in low supply as aquatic overwintering is a result of a temperature-dependent decline of food supply. Because American bullfrogs have been identified to have higher levels of astrocyte glycogen during overwintering months (McDougal et al., 1968), I predict that glycogenolysis localized within the tissue is responsible for providing the primary fuel source of this glycolytic network. If the CA respiratory

motor network is fueled by astrocytic glycogen, I would expect results showing ischemia-tolerance with an improvement in prolonged activity in oxygen and glucose deprivation (OGD) compared to the control. If I determine CA brainstems to be ischemia-tolerant, blocking glycogenolysis during exposure to OGD should result in energetic failure.

Pitfalls and alternative explanations: **(1)** Despite WA response to hypoxia showing parallels with mammalian energetic failure in extracellular recordings, cessation of activity is believed to be a result of a neuroprotective strategy that inhibits neuronal activity through noradrenergic signaling in response to severe hypoxia in American bullfrogs (Fournier et al., 2007; Fournier & Kinkead, 2008). This has been assessed in further detail recently by our lab, where we concluded that noradrenergic signaling and energy-sensing mechanisms are not involved in a neuroprotective shutoff (Adams et al., 2021). **(2)** Although our methodological approach to hypoxia superfusing is sufficiently hypoxic to result in metabolic failure in WA control frogs, it is possible that the environment is not entirely anoxic as trace amounts of O_2 can still exist in the tissue. Therefore, persistent activity could potentially be explained by enhancing mitochondrial efficiency at very low oxygen tensions. This “efficient mitochondria” hypothesis will be tested by blocking the electron transport chain with 1mM sodium cyanide (NaCN) (Adams et al., 2021; Cheng et al., 2021). I expect to see continuous rhythmic activity after NaCN application as my initial hypothesis suggests that mitochondrial activity is absent in this model during hypoxia and OGD.

Specific Aim 2: Identify costly mechanisms that are altered to increase efficiency within the network.

A shift to an alternative fuel supply would most likely result in a significant net decrease in free energy availability, which requires enhanced efficiency of costly physiological processes to persevere the limited ATP supply and network function. One costly form of network function involves synaptic communication between neurons using NMDA receptors (NMDARs),

glutamate-gated ion channels that allow Na^+, Ca^{2+}, and K^+ to trigger action potentials in the postsynaptic neuron (Madison et al., 1991). Indeed, NMDA receptors are implicated in many hypoxia/ischemia models because Ca^{2+} induces cell death (termed “excitotoxicity”) due to influx from NMDARs (Wu & Tymianski, 2018). In addition, NMDARs represent a likely energetic sink within healthy neural circuits. Maintaining a stable membrane potential through ion regulation during ongoing network function is a highly expensive process (Bordone et al., 2019). Primary contributors to maintaining stable ion gradients are active transporters that hydrolyze ATP to pump ions across the cell membrane. The primary active transporter involved in maintaining the Ca^{2+} gradient across the plasma membrane in neurons is the plasma membrane Ca^{2+} ATPase (PMCA) which transports 1 Ca^{2+} ion per ATP hydrolyzed (Stafford et al., 2017). By calculating energy expenditure through Gibb’s free energy equation, the free energy required for Ca^{2+} active transport seems to be more than 3-times greater compared to Na^+ transport per mole of ions through the Na^+-K^+ ATPase (See Appendix A). My preliminary data shows that application of D-AP5, an NMDAR antagonist, results in reduced population burst amplitude from extracellular nerve recordings from the network (Figure. 2). This suggests that synaptic transmission *via* NMDA receptors generates network output in this system, and the subsequent Ca^{2+} load, present a significant energetic burden, making a logical component that may be adjusted to improve efficacy of network function during hypoxia. Given this information, I hypothesize that improved hypoxia tolerance following CA involves modifications to synaptic transmission such that NMDAR expression and/or function reduces Ca^{2+} influx. Specifically, I expect NMDA receptors will be downregulated and/or replaced with Ca^{2+} impermeable neurotransmitter receptors. I will test this by conducting experiments that assess the hypoxic response in WA and CA respiratory motor circuits exposed to a block of NMDARs. To directly assess NMDAR function (current density, kinetics, Ca^{2+} permeability) in single cells, I will test the function of NMDAR currents in CA and WA neurons using whole-cell voltage clamp electrophysiology.

Aim 2a: Determine if NMDAR block prolongs functional activity in hypoxia.

I conducted experiments that identify NMDAR prevalence in WA and CA neural circuits through pharmacological block. NMDAR antagonist, D-AP5, was applied to brainstems to observe changes in output tone, where changes in relative amplitude after stability in D-AP5 was determined as sensitivity to NMDAR block. To test for a change in hypoxia tolerance, WA brainstem preparations were exposed to hypoxia following D-AP5 stability. Hypoxia sensitivity was determined by time until metabolic failure and compared to WA brainstem controls to observe potential improvements.

Figure 2. Respiratory circuit output is normally largely determined by NMDA receptor neurotransmission. Preliminary data showing WA circuit output sensitivity to NMDAR block via D-AP5 represented by change in stable burst amplitude.

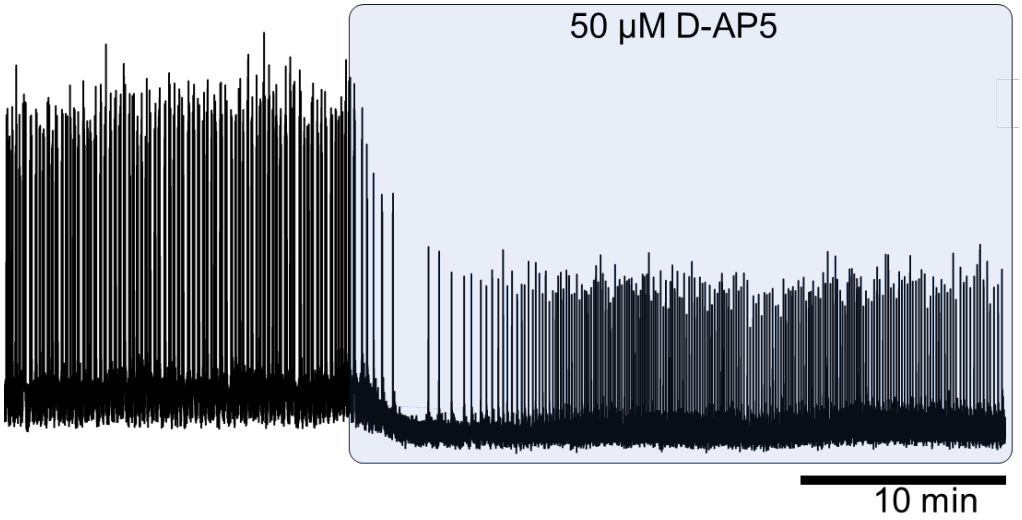

Aim 2b: Compare Ca permeabilities between WA and CA neurons.

I determined changes in Ca^{2+} permeability in neurons between treatment groups through whole-cell voltage clamp methods and interpolating the reversal potential (E_{rev}) of neurons exposed to varying Ca^{2+} concentrations. E_{rev} of an ion channel is defined as the voltage at which current flowing through the channel reverses direction due to the electrochemical forces and is determined by the ion selectivity of the channel. Therefore, the E_{rev} of the ion channel ($E_{channel}$) provides a direct measure of ion selectivity. I determined changes in NMDAR Ca^{2+} permeability

between CA and WA neurons by shifts in E_{rev} in solutions with different Ca^{2+} concentrations. This method can be used to calculate Ca^{2+} permeability relative to Na^{+} ions (*i.e.* permeability coefficients, P_{Ca}/P_{Na}; Jatzke et al., 2002; Lewis, 1979). However, I only relied on population data of E_{rev} shifts to conclude permeability.

Primary Expected Results

Aim 2a: My hypothesis suggests NMDAR function and/or expression will decrease in CA to increase neuronal efficiency, so I expect to observe a lower sensitivity to NMDAR block in CA brainstem output amplitude compared to WA brains. Furthermore, if CA brainstems decrease NMDA receptor function, I should be able to mimic this in WA brainstems with D-AP5, where the expected outcome would be an increased duration of functional activity in WA brainstems when exposed to hypoxia. **Aim 2b**: If there is a reduced sensitivity to D-AP5 in Aim 2a, I would also expect to see an overall reduction in dendritic and somatic Ca^{2+} influx in CA respiratory motor neurons, as NMDARs were likely to be downregulated. If there is no change in sensitivity to D-AP5 at the network level, it would suggest that receptors have not been downregulated, but that NMDARs have been replaced by receptors that are less permeable to Ca^{2+}.

Pitfalls and alternative explanations: **(1)** Although NMDAR-induced excitotoxicity is associated with hypoxia-intolerant neuron models, there may not be a significant time difference in energetic failure in the extracellular D-AP5 experiments in control preparations. I expect this outcome, potentially, because I believe many energetic inefficiencies could be corrected following winter, with no single mechanism being sufficient to explain the entire improved hypoxia tolerance response. However, the well-supported association with NMDAR-induced excitotoxicity existing in literature keeps this specific question worthwhile regardless of the outcome. **(2)** A significant change in sensitivity of the network to NMDAR block may not exist when comparing burst amplitude changes in CA and WA brainstems upon D-AP5 exposure. This would suggest that NMDARs as a whole are expressed and functioning similarly to the WA

neurons. This does not exclude the possibility that other variables are resulting in a reduced Ca^{2+} permeability through NMDAR modifications. Indeed, D-AP5 blocks both calcium-permeable and impermeable receptor subtypes. Therefore, if calcium permeability changes without decreasing total receptor density, this outcome would manifest as “no change” in motor burst sensitivity.

CHAPTER III: METHODS

Animal Husbandry and Ethical Approval

All protocols have been approved by IUCUC at the University of North Carolina at Greensboro (Protocol #19-006). Female American bullfrogs (*Lithobates catesbeianus*) were acquired from Rana Ranch (Twin Falls, ID, USA) and housed in plastic tubs with dechlorinated and aerated water in a light/dark cycle of 12/12 hours. Control frogs were placed in tubs at room temperature (22°C), where they had access to wet and dry areas and were fed pellets once per week. Frogs were randomly assigned to one of two groups (control or hibernation). Control frogs were acclimated to lab conditions for at least one week before experiments. To simulate overwintering conditions, we placed another set of animals in low-temperature incubators (Thermo Fisher Scientific, Waltham, MA, USA). In this type of temperature acclimation manipulation, frogs have been shown to undergo metabolic suppression consistent with hibernation (Tattersall & Ultsch, 2008). Therefore, we refer to this group as “hibernation” in this study. The temperature inside the incubator was gradually reduced from 20-22°C to 4°C over 7 days. Upon reaching 4°C on day 7, screens were placed directly below water level to impede access to the surface, and frogs were kept at 4°C for 33±2 days before use in experiments.

Dissection

Brainstem-spinal cord preparations were generated using standard methods from our lab (Adams et al., 2021). Frogs were deeply anesthetized with isoflurane (1 mL) in a sealed container until toe-pinch reflex was lost, which was followed by decapitation. The head was submerged in chilled artificial cerebral spinal fluid (aCSF) containing (in mM) 104 NaCl, 4 KCl, 1.4 $MgCl_2$, 7.5 D-glucose, 1 NaH_2PO_4, 40 $NaHCO_3$, 2.5 $CaCl_2$ (Santin & Hartzler, 2013), all purchased Fisher Scientific (Waltham, MA, USA). The aCSF was constantly bubbled with 98.5% O_2 and 1.5% CO_2 maintaining a pH of ~7.85-7.95. The skull was quickly removed, the forebrain was crushed, the brainstem-spinal cord was carefully removed from the bones, and the dura

was removed exposing cranial nerve roots. Following the dissection, all preparations were maintained at room temperature, (22±1^{o}C).

Extracellular Nerve Root recordings

Brainstem- spinal cord preparations were pinned ventral side up in 6 ml Petri dishes coated with Sylgard (Dow Inc. Midland, MI, USA) and continuously superfused with aCSF gassed with 98.5% O_2/1.5% CO_2 using peristaltic pumps (Watson Marlow, Falmouth, CNL, UK). Borosilicate glass pipettes pulled with a horizontal puller (Sutter Instruments, Novato, CA, USA) were carefully broken at the tip and fire-polished to ensure a tight seal between the tip of the pipette and nerve roots. Rhythmic motor output from the respiratory network was then recorded from two of the following motor nerves using suction electrodes: vagus (cranial nerve X; CN X), trigeminal (CN V), or hypoglossal (Figure 3A). Respiratory motor bursts were characterized by showing near-synchronous activity on both nerves, with a ramp-like increase and decrease over ~1s (Figure 3B, CN X only). Both nerves in each experiment showed the same response to all treatments. Raw extracellular outputs were integrated and rectified. All treatments affected both nerves similarly in all experiments. Small noise artifacts (caused by touching the rig, air bubble in inlet line, *etc.*) sometimes occurred in silent preparations and were easily discerned by narrow integrated burst widths relative to the 1s respiratory burst and were ignored in analysis. Extracellular signals were amplified (x100), filtered (low-pass, 1000 Hz; high-pass, 10 Hz) using an amplifier (A-M Systems 1700 amplifier, Sequim, WA, USA), and digitized with PowerLab 8/35 (ADInstruments, Dunedin, New Zealand). The raw signal was sampled at 1k/s recorded, rectified, and integrated using LabChart 8 software (ADInstruments, Dunedin, New Zealand). All preparations produced rhythmic network activity following dissection and no preparations were excluded from the data set.

Figure 3. In vitro brainstem recordings. (A) Brainstem-spinal cord preparation with nerve-roots innervated by rhythmic motor pools that produce fictive breathing output labled (hypoglossal, SNII; glossopharyngeal vagus complex, CNX; trigeminal, CNV). (B) Rhythmic lung bursts recorded on CNX nerve root.

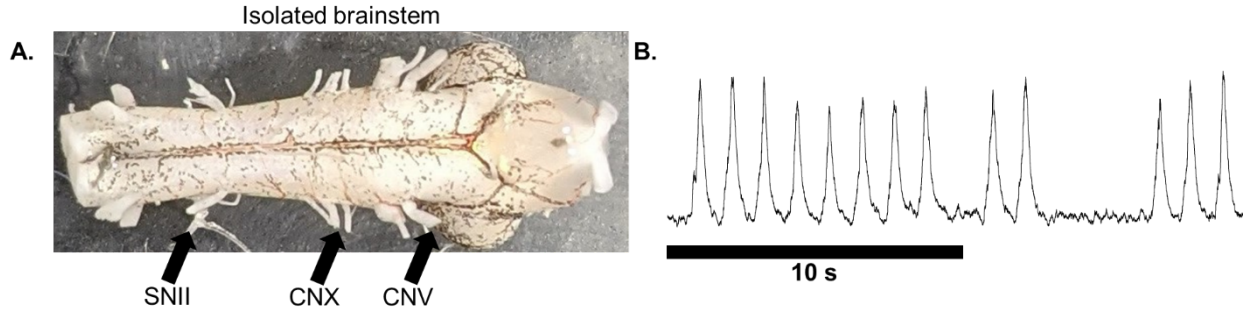

Cell Labeling and Slice Preparation

Brainstem-spinal cords were pinned and superfused with oxygenated aCSF (See "Extracellular Recordings") with the vagal nerve (4th root) isolated from the glossopharyngeal vagus complex and attached to fire-polished borosilicate glass pulled from a horizontal pipette puller (Sutter Instrument, Novato, CA, USA). aCSF was removed from the pipette and replaced with 3000 MW tetramethylrhodamine dextran dye (Invitrogen, Waltham, MA, USA) and allowed a minimum of 2 hours to diffuse to the soma on each hemisphere. The brainstem-spinal cord preparations were then sliced at a width of 300 μM using a vibratome (Pelco, Fresno, CA, USA).

Brainstem-Spinal Cord Experimental Protocols

All protocols were carried out on brainstem-spinal cord preparations at room temperature, 22±1°C. All preparations included in this study produced rhythmic motor output associated with lung breathing (Tattersall & Ultsch, 2008). Experimental protocols were performed 4 hours following decapitation to ensure a stable baseline for all recordings.

Severe hypoxia

Following a baseline recording in control gas mixture (98.5% O_2, 1.5% CO_2) severe hypoxia was induced by superfusing the brainstem-spinal cord with aCSF bubbled with 98.5% of N_2 and 1.5% of CO_2. The preparations (control, n=8; hibernation, n=8) were exposed to severe hypoxia treatment for 4 hours and then all preparations but one control was reoxygenated by

superfusing control aCSF for a one-hour recovery period. Oxygen levels in the chamber were measured with a luminescent dissolved oxygen sensor (LD0101; Hach Company, Loveland, Colorado, USA). Under the conditions of our experiment, changing the solution to 98.5% N_2/1.5% CO_2 led to a chamber O_2 level of 2% after ~10 minutes. Winmill et al. (2005) measured tissue Po_2 under similar experimental conditions that we used here (chamber volume, flow rate, N_2 replacing O_2, adult brainstems) and determined that tissue Po_2 is severely hypoxic and likely anoxic (Winmill et al., 2005).

Oxygen and Glucose Deprivation (OGD)

For OGD, the D-glucose used in aCSF was replaced with equimolar sucrose (7.5 mM, Fisher Scientific, Waltham, MA, USA) and bubbled with 98.5% N_2 and1.5% CO_2. Following a baseline recording in control conditions, preparations (control, n=8; hibernation, n=6) were exposed to OGD for 2 hours. Preparations were then superfused with control aCSF during a 1 hour recovery period.

Sodium cyanide and Iodoacetate exposure

To ensure complete inhibition of mitochondrial respiration and glycolysis during OGD in hibernation preparations, we prepared (A) an OGD solution containing 1 mM Sodium Cyanide (CN) to inhibit complex IV of the electron transport chain (Acros Organics, Morris Plains, NJ, USA) (Cheng et al., 2021); (B) an OGD+CN solution containing 1mM Iodoacetate to inhibit glycolysis (Acros Organics, Morris Plains, NJ, USA) (Adams et al., 2021; Lutas et al., 2014). Preparations from the hibernation group (n=5) were first exposed to CN under OGD conditions for 1 hr. Since CN did not stop network function, we then exposed the preparations to Iodoacetate in OGD+ cyanide until network failure was observed. Because Iodoacetate induces an irreversible inhibition of glyceraldehyde 3-phosphate dehydrogenase (Schmidt & Dringen, 2009), recovery was not expected and these preparations were not washed out with control aCSF.

DAB exposure

In this protocol glycogen phosphorylase, the rate-limiting enzyme of glycogenolysis, was inhibited by 250 μM of 1,4-dideoxy-1,4-imino-D-arabinitol (DAB, Cayman, Ann Arbor, MI, USA) to investigate if local glycogen stores supported network function (Walls et al., 2008). Following baseline recordings in control aCSF, hibernation preparations (n=5) were exposed to OGD in the presence of DAB for two hours, which was followed by superfusion with control aCSF during 1 hour for recovery.

NMDAR Tone Experiments

50 μM D-AP5 dissolved in aCSF was applied to both WA and CA brainstems (WA, n=8; CA; n=8) after stable baseline amplitude was recorded from the hypoglossal nerve (SNII). Hypoxia was administered once the rhythmic output established a new baseline (~1 hour). Using D-AP5 as an NMDAR antagonist has been shown to be feasible for these experiments as the data shows persistent activity upon D-AP5 exposure allows for a recording of a stable amplitude during these experiments (Figure 2).

Single-Cell NMDAR Activation Experimental Protocol

Slices were superfused with extracellular solution (76.5 mM NaCl, 2.2 mM KCl, 7.5 mM D-Glucose, 10 mM HEPES, 300 μM $CdCl_2$, 20 mM TEA-Cl, 250 μM TTX, 10 μM DNQX) with two different Ca^{2+} concentrations for high Ca^{2+} (10 mM $CaCl_2$, 60 mM Sucrose) and low Ca^{2+} (1 mM $CaCl_2$, 89 mM Sucrose), with sucrose added to maintain a consistent osmolarity (330 mOsm). Extracellular solution was oxygenated by bubbling 98.5% O_2 and 1.5% CO_2 in superfusion reservoirs. $MgCl_2$ was excluded to prevent hyperpolarized NMDAR Mg^{2+} block. Patch pipette solution (76.5 mM K-gluconate, 10 mM D-glucose, 10 mM HEPES, 1 mM Na_2-ATP, 0.1 mM Na_2-GTP, 2 mM $MgCl_2$, 30 mM TEA-Cl) was designed with Na^+ and K^+ concentrations equal and opposite to the extracellular solution to allow a reversal potential at 0 mV without Ca^{2+} presence (assuming no ion selectivity between Na^+ and K^+ ions) as seen in

previous NMDAR reversal potential papers (Jatzke et al., 2002). A borosilicate pipette pulled with a tip diameter of ~5 μL was filled with NMDA (1 mM) and glycine (10 μM) dissolved in recording solution and driven by a Picospritzer II (General Valve Corporation, Fairfield, NJ, USA) to activate NMDARs on the soma of labeled vagal motoneurons (Figure 4). Glycine is an obligate co-agonist of the NMDAR, but did not elicit any responses when applied alone (Figure 3). NMDAR E_{rev} was recorded by a 13-step voltage clamp protocol with a Δ5 mV ranging between -20 mV and 40 mV with the exception of 3 recordings that had a more depolarized E_{rev} that was recorded between -40 mV and 20 mV (WA, n=16; CA, n=16). NMDAR desensitization was recorded by puffing at a rate of 0.5 Hz for a total of ten pulses at -20 mV (WA, n=12; CA, n=14). Hypoxia was applied to brain slices by bubbling extracellular solution with 98.5% of N_2 and 1.5% of CO_2 in the superfusion reservoir and exposed for ~5 minutes before recording. All desensitization and single activation amplitude and kinetics experiments were performed on neurons held at -20 mV.

Figure 4. Respiratory motor neurons are sensitive to NMDA puffing in Mg2+-free aCSF. NMDA (500 μM) dissolved in the same saline as the extracellular solution was applied by a Picospritzer II at 10 psi for 10 ms. (A) Image of a hypoglossal neuron being recorded in whole-cell patch clamp with a spritzing pipette aimed at recorded cell (Magnified 400x). (B) Trace recording of a cell in voltage clamp held at -70 mV showing current response to NMDA application. (C) Recording of a cell in voltage clamp showing no response to glycine (10 μM) puff.

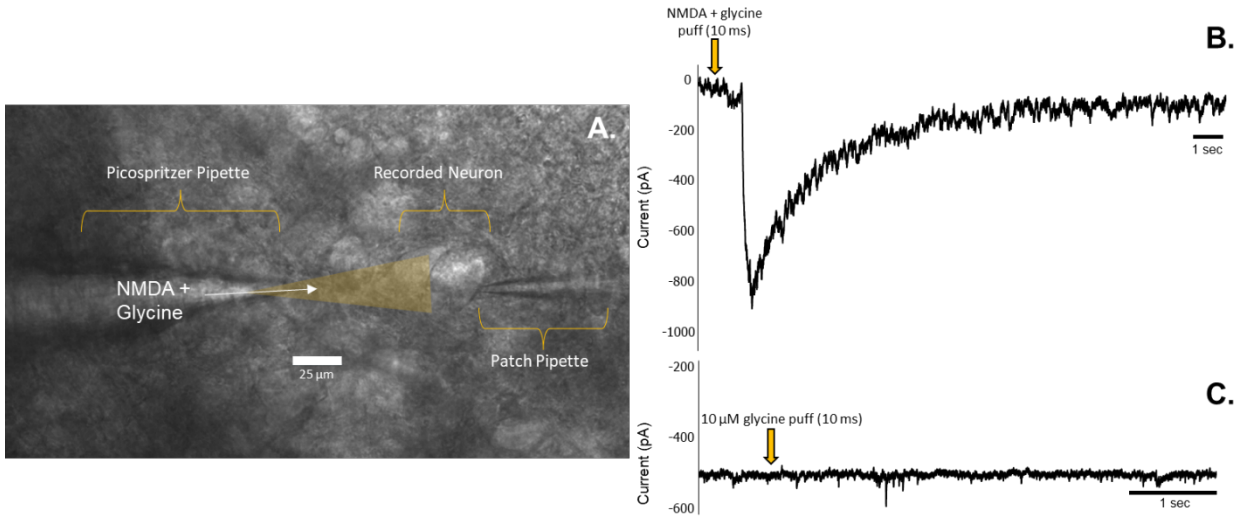

Data Analysis

Extracellular Motor Output

Aim 1: Baseline frequency of the respiratory network (activity represented in Figure 5) was determined by quantifying large-amplitude lung bursts within the 10 min preceding a treatment. During the treatment, frequency was analyzed in 5 min bins throughout the recording period and normalized to baseline to account for individual variation in initial burst frequency. Network failure time is reported as the time until rhythmic activity stopped in each condition. Analyses were not performed blinded.

Aim 2: Baseline amplitude was determined by average amplitude of large-amplitude lung bursts that have been integrated and rectified selected in a 5-minute window prior to D-AP5 application, amplitude with NMDAR block was analyzed at a similar time window after stabilization in D-AP5. Absolute amplitude values were not considered during analysis due to high variability of burst amplitude that is not dependent on relevant factors. Therefore, amplitude changes invoked by D-AP5 relative to stable amplitude were determined during analysis. Peak amplitude was determined using the Peak Analysis extension in LabChart (ADInstruments, Dunedin, New Zealand), with false positives removed manually.

NMDAR Ca^{2+} Permeability

Relative Ca^{2+} permeability was determined by the degree of shift in the NMDA E_{rev} based on the mean data of the population. The change in current (ΔI) was measured between the holding current and the NMDAR-activated current at each voltage step, plotting the current-voltage relationship, and interpolating E_{rev} through the x-intercept of the line of best fit from 3-5 plot points near the intercept where V=0 mV. Series resistance (R_s) was calculated at each step to correct for holding voltage error induced by R_s. Peaks were measured using the Peak Analysis extension in LabChart. Averaging/decimation at 0.05-0.1 ms was applied to the traces

prior to peak analysis to filter out high-frequency non-NMDAR associated spontaneous activity. This level of filtering was chosen due to minimal alteration to the amplitude.

Divalent cations can adhere to the outer edge of cell membranes and introduce an electric field, making the apparent voltage at the membrane more depolarized with increased divalent cations, deemed “charge screening” (Hille, 2001). However this Ca^{2+} concentration-dependent bias does not seem to affect our data interpretation since E_{rev} data on Ca^{2+}-impermeable kainite receptors from Jatzke *et al*. showed a <2 mV difference between the Ca^{2+} concentrations we used (Jatzke et al., 2002).

Single-Cell NMDAR Activation

ΔI was measured using similar methods as the NMDAR Ca^{2+} permeability methods. Desensitization amplitude was measured by using the recovered current at each step interval as the baseline value for the proceeding pulse amplitude. Tau was determined between 90% and 10% of the peak height and calculated using the Peak Analysis tool in LabChart.

Statistical analysis

For all tests, significance was accepted when $p < 0.05$. For all experiments, raw data are shown either as single circles, lines across time, or lines representing ‘before’ and ‘after’ responses for individual data points.

Extracellular Data

Differences in the time until network failure due to 2% O2 or to OGD in control preparations versus after hibernation preparations were compared by a Welch’s t-test. The effect of IAA on OGD+CN hibernation preparations was compared with hibernation preparations in OGD alone at similar time points in the experiment (60 and 70 min). This analysis served two purposes: it allowed us to determine whether CN affected burst frequency independently of OGD, and it also ruled out the possibility that IAA stopped network activity due to time effects alone. This analysis was carried out with a two-way ANOVA and Sidak’s multiple comparison

test. Comparison of the time until network failure in controls, after hibernation and after hibernation + DAB was evaluated using one-way ANOVA. For these variables, the differences among the averages were evaluated using Tukey's multiple comparisons test. The proportion of preparations recovering/not in the recovery period following 2% O2 or OGD were compared using Fisher's exact test. Relative changes in amplitude tone from D-AP5 exposure between control and hibernation preparations were compared *via* an unpaired t-test.

Patch-Clamp Data

Unpaired t-tests were used to compare warm vs. cold effects to NMDAR activated current amplitude and desensitization. For data pairing normoxic and hypoxic responses, paired t-tests were used. Analysis of entire desensitization response was analyzed through a two-way ANOVA. This test was also used to analyze the changes in reversal potentials from low and high Ca^{2+} concentrations between WA and CA vagal motoneurons. This was used as testing for significant interaction is necessary to determine if the state of the animal (WA or CA) affects the response to Ca^{2+} E_{rev}.

CHAPTER IV: TRANSFORMING A NEURAL CIRCUIT TO FUNCTION WITHOUT OXYGEN AND GLUCOSE DELIVERY (AIM I)

Bueschke, N., Amaral-Silva, L. do, Adams, S., & Santin, J. M. (2021). *Current Biology*, *31*(24), R1564–R1565.

Disruptions in the delivery of oxygen and glucose impair the function of neural circuits, with lethal consequences commonly observed in stroke and cardiac arrest. Intense focus has been placed on understanding how to overcome neuronal failure during energy stress. Important insights into neuroprotective strategies have come from studies of evolutionary adaptations for survival in hypoxic environments, such as those seen in turtles, naked mole-rats, and several other animals (Larson et al., 2014). Amphibians are not usually numbered among 'champion' hypoxia-tolerant vertebrates, yet here we demonstrate a massive conditional increase in the capacity of a neural circuit to produce activity following oxygen and glucose deprivation in adult bullfrogs. Rhythmic output from a brainstem circuit failed following minutes of severe hypoxia and simulated ischemia; however, after hibernation this network produces patterned activity for ~3.5 hours during severe hypoxia and ~2 hours in ischemia. This remarkable improvement was supported by a switch to brain glycogen to fuel anaerobic glycolysis, a pathway thought to support neuronal homeostasis for only a few minutes during ischemia (Allen et al., 2005). These results reveal that circuit activity can exhibit dramatic metabolic plasticity that minimizes the need for ATP synthesis and these findings represent the greatest range in hypoxia tolerance within a vertebrate neural network. Uncovering the rules that allow the brain to flexibly run only on endogenous fuel reserves will reveal new insights into brain energetics, circuit evolution, and neuroprotection.

To address the response of a complete motor circuit to reduced ATP turnover, we exposed the brainstem respiratory network from American bullfrogs to severe hypoxia (~2% O_2). Severe hypoxia typically induced hyperexcitability followed by silence within a few minutes

(Figure 5A), a response outwardly similar to that seen in mammalian networks with high energetic demands (Somjen, 2001). In contrast, under the same experimental setting, animals removed from a simulated overwintering environment produced network activity for an average of 210 minutes (range 137-240 min) (Figure 5B; Figure 6A). These results led us to test whether networks transform to resist oxygen and glucose deprivation (OGD), an *in vitro* ischemia mimetic. During OGD, control preparations operated for ~4 minutes, while hibernator networks continued for ~116 minutes (range 103-120 minutes), a ~30-fold increase in time until cessation of electrical activity (Figure 5C; Figure 6B). These data show the frog brainstem exhibits metabolic plasticity that dramatically prolongs function in the absence of oxygen or glucose delivery.

Network function without aerobic metabolism in hibernators was verified by exposing brainstems to OGD plus 1 mM sodium cyanide (CN), ensuring inhibition of mitochondrial respiration (Adams et al., 2021). After 1 hour of OGD+CN, burst frequency was comparable to OGD alone (Figure 5D). We then inhibited glycolysis using 1 mM iodoacetate to test whether glycolysis supported network function. Iodoacetate in the presence of ODG+CN quickly led to hyperexcitability and then network silence (Figure 5D). Therefore, hibernation induces the ability for glycolysis to fuel network function with only local fuel stores.

Glial cells store glycogen in mammals and amphibians (Rossi et al., 2007; Samosudova et al., 2010) but are generally thought to fuel network activity for only a few minutes (Allen et al., 2005). However, brain glycogen increases in frogs during winter (McDougal et al., 1968), suggesting the network can switch to glycogen as an alternative fuel source. Thus, we examined the effects of inhibiting glycogen phosphorylase, which catalyzes the rate-limiting step of glycogenolysis, using 1,4-dideoxy-1,4-imino-D-arabinitol (DAB; 250 μM). In the presence of DAB, hibernation preparations became hyperexcitable and stopped after ~25 min of ODG, significantly shorter than the ~116 min with OGD alone but longer than controls (Figure 5E). In addition, no control preparations recovered following restoration of oxygen and glucose,

whereas five of six hibernators resumed near-normal rhythmic activity. However, when hibernation preparations were treated with DAB, we did not observe recovery of activity (Figure 6C-D).

Circuit function requires ongoing ATP production through aerobic metabolism due to the high cost of electrical signaling (Harris et al., 2012). Indeed, most animals succumb to severe hypoxia and ischemia within minutes, or in the case of inherently hypoxia-tolerant species, use adaptations to oppose ATP depletion and tissue damage (Larson et al., 2014). It was therefore surprising that a complete network with high aerobic demands (Adams et al., 2021) (Figure 5A) could undergo transformation to produce motor activity for hours without aerobic metabolism or glucose delivery. Thus, we reveal that adult vertebrate circuits can exhibit metabolic plasticity, switching between aerobic and highly glycolytic states to support network function even without glucose delivery.

Although we identified glycogenolysis as a requirement of metabolic plasticity (Figure 5D), we speculate that additional network adjustments must contribute. Circuit activity represents a balance between ATP supply and the energetic cost largely associated with excitatory synaptic transmission (Rangaraju et al., 2014). Given that anaerobic glycolysis produces far less ATP compared with aerobic metabolism, we reason that excitatory synaptic function must become substantially more efficient otherwise glycolysis/glycogenolysis could not support network activity for as long as we observed. Therefore, along with enhancing the use of alternative fuels most likely supplied by glia (Rossi et al., 2007), the energy used for synaptic vesicle cycling and ion regulation may be reduced as low as network function permits.

Bullfrogs overwinter under water which dramatically lowers blood O_2 due to their sole reliance on gas exchange through the skin (Tattersall & Ultsch, 2008). Therefore, metabolic plasticity in the respiratory network may serve to restart breathing upon emergence from hibernation when O_2 is otherwise below the aerobic requirement of circuit function, a problem compounded by metabolic rate increases associated with rising body temperature. More

broadly, these results imply circuits may not always exist in their most energetically efficient state, which adds a layer of complexity to the understanding of circuit evolution. Circuit function is thought to reflect natural selection for optimized information transfer relative to ATP consumption (Rangaraju et al., 2014). However, the large capacity for metabolic plasticity we observed brings into question the advantage of network designs with such high metabolic requirements: Why settle on an expensive network if less costly possibilities achieve the same function? Do networks with ultra-high efficiency come at a cost? Can other networks transition to function during bouts of low ATP synthesis? At its core, metabolic plasticity here seems to represent the overarching goal for human neuroprotection: preemptively transforming circuits to avoid a collapse in integrity during an energy crisis. Therefore, learning how to modify circuits to function during oxygen and glucose deprivation may uncover new principles for both circuit energetics and neuroprotection alike.

Figure 5. Dramatic improvement in circuit function during severe hypoxia (2% O_2) and O_2-glucose deprivation (OGD) after hibernation. (A) Simplified schematic of the in vitro bullfrog brainstem preparation and activity produced by the respiratory network that generates breathing. Motor output is produced by a lung breathing rhythmgenerating network (L) that drives motor neuron discharge (MN; cranial nerve X recorded here). The integrated neurogram shows the typical response to severe hypoxia, involving hyperexcitability and, shortly after, network silence. (B) Representative data trace of integrated neurograms and mean time until silence of network output, illustrating the striking increase in duration of respiratory motor function during severe hypoxia following hibernation (control, n = 6; hibernation, n = 8). (C) Representative data trace of the OGD response before and following hibernation. (D) A representative neurogram of a hibernation preparation exposed to cyanide (CN) in OGD for 60 minutes to inhibit aerobic metabolism followed by application of iodoacetate (IAA) to inhibit glycolysis (left). The plot on the right shows that at 60 minutes OGD+CN has a similar frequency to OGD alone, indicating that network function occurred without aerobic respiration. However, frequency falls following IAA exposure, demonstrating glycolytic support of network activity. (E) Representative network responses to OGD in frogs after hibernation, and after hibernation plus treatment with DAB to inhibit glycogen phosphorylase. Mean data on the right show the time until network failure during OGD in control (left, green, n = 8), hibernation (middle, blue, n = 6) and hibernation + DAB (right, light blue, n = 5). Dots represent data points from each preparation in individual experiments, horizontal bar is drawn at the mean, and error bars are S.E.M.

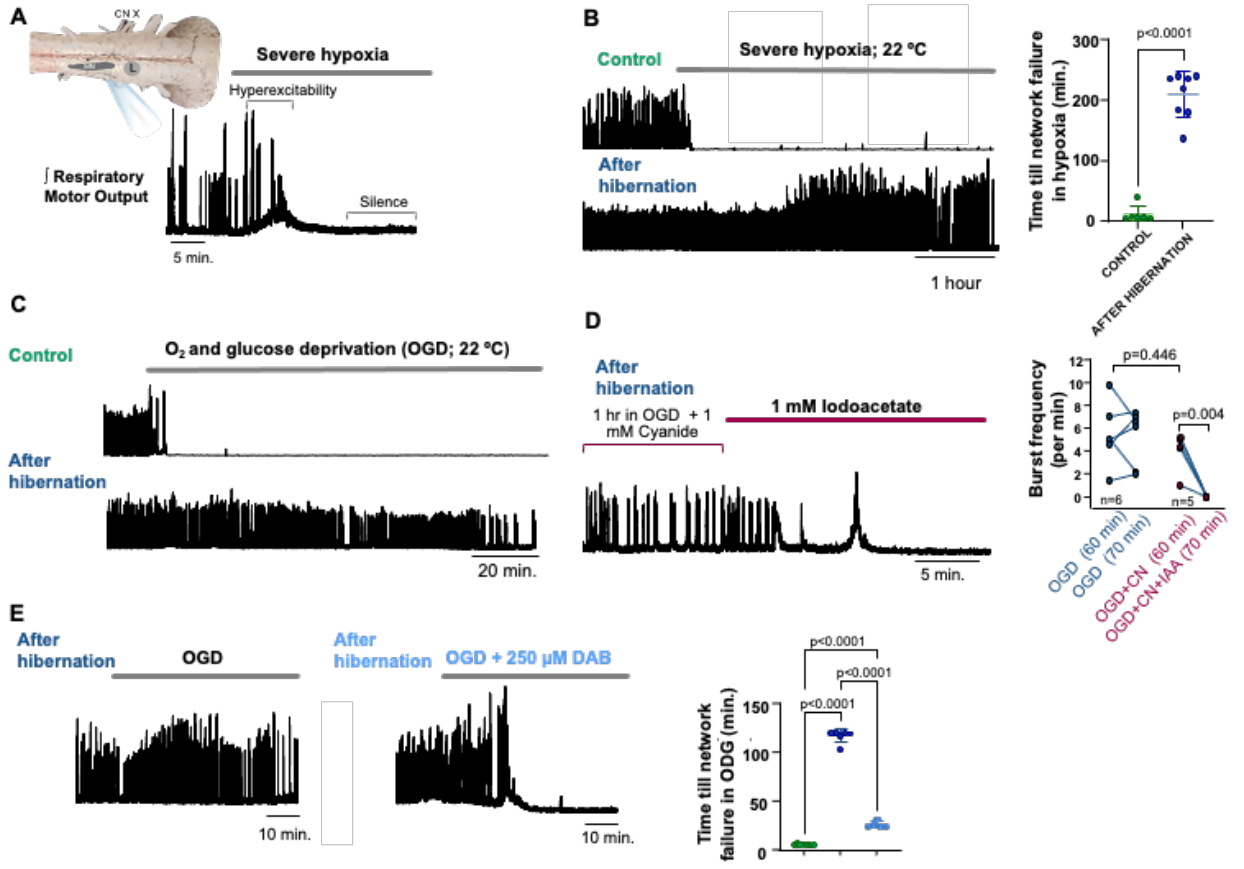

Figure 6. Time course of burst frequency during hypoxia and oxygen-glucose deprivation (OGD). (A-B) Mean data (left panel) and responses of individuals (right panel) network burst frequency throughout the full duration of anoxia (A) or OGD (B). (C) Number of preparations recovering activity following the 4 hour treatment with severe hypoxia in control (2/6) and post-hibernation conditions (7/7). (D) Number of preparations recovering activity following the 2 hour treatment with oxygen and glucose deprivation (OGD) in control (0/8), hibernation (5/6), and hibernation + glycogen phosphorylase inhibitor (250 μM DAB) (0/5) conditions.

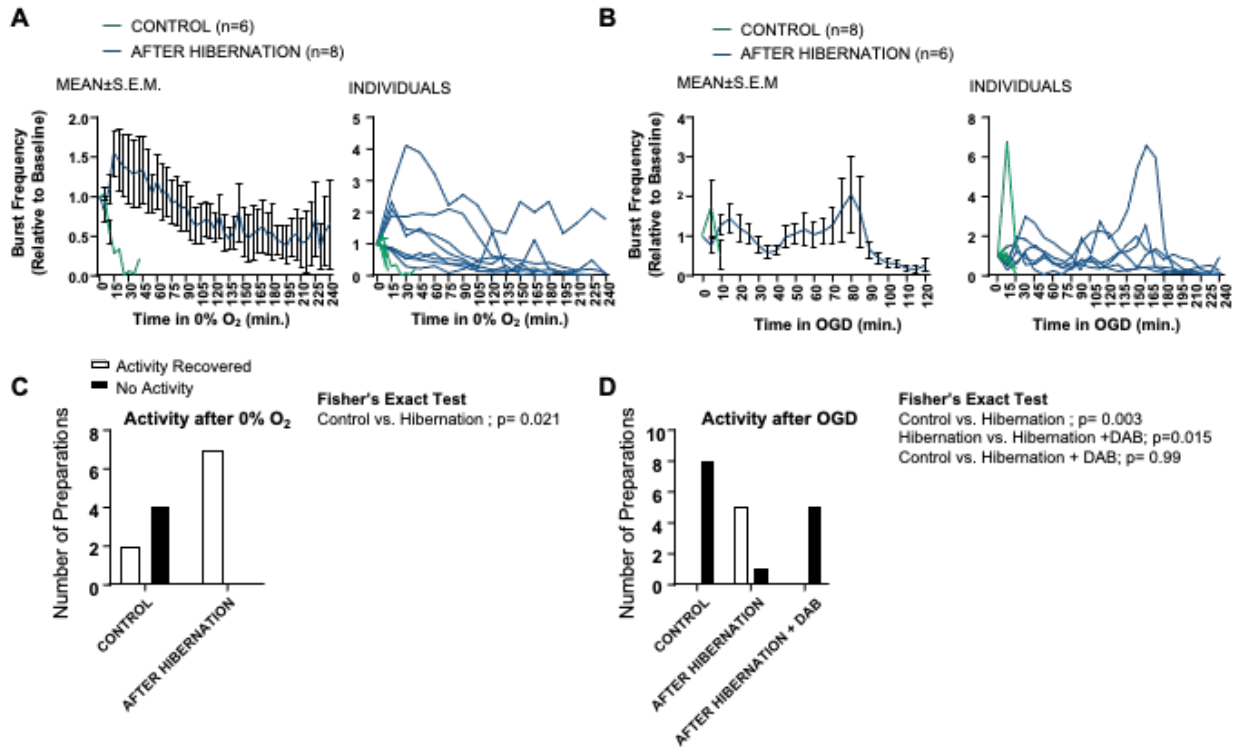

CHAPTER V: SWITCHING TO CA2+ IMPERMEABLE NMDA-GLUTAMATE RECEPTORS INDUCES HYPOXIA TOLERANCE OF NEURAL CIRCUIT FUNCTION (AIM II)

Abstract

Hypoxia and ischemia lead to neuronal hyperexcitability followed by a rapid loss of function and cell death. In contrast, adult bullfrogs have the remarkable ability to switch into a brain state that prepares them to maintain neural function during severe hypoxia as they emerge from hibernation. NMDA receptors (NMDARs) are Ca^{2+}-permeable glutamate receptors that drive pathological loss of homeostasis during ischemia. Therefore, we hypothesized that hibernation improves neuronal performance in hypoxia by reducing the contribution of NMDARs to network function. To test this, we recorded rhythmic motor output in a brainstem network with a large contribution from NMDAR transmission, the brainstem respiratory network. Contrary to our expectations, hibernation and hypoxia do not alter the NMDAR tone, nor do they affect the amplitude and kinetics of NMDAR currents. Instead, we find that hibernation greatly reduces Ca^{2+} permeability of NMDARs and enhances desensitization during repetitive stimulation in association with changes to the NMDAR subunit profiles in single neurons. NMDARs normally contribute to motor hyperexcitability in severe hypoxia, but after hibernation, networks show healthy function and no evidence of hyperexcitability despite a normal NMDAR tone. Therefore, reduced Ca^{2+} permeability and enhanced desensitization of NMDARs constrain network excitability during hypoxia while maintaining their normal contribution to motor function. These findings reveal plasticity that reduces the cost of synaptic transmission before an energetic insult to improve neuronal function and survival.

Introduction

The brain requires high rates of ATP synthesis relative to most tissues to generate healthy function (Bordone et al., 2019). In circuits that use excitatory synaptic transmission, the sudden loss of oxygen triggers hyperexcitability that leads to ion dysregulation and cell death

(Buck & Pamenter, 2018). A key contributor to excitotoxicity involves the activation of NMDA glutamate receptors (NMDARs), causing massive Ca^{2+} influx that induces reactive oxygen species (ROS), pro-death signaling pathways, and mitochondrial damage (Wu & Tymianski, 2018). Ca^{2+} influx saturates intracellular buffering systems (Szydlowska & Tymianski, 2010; White & Reynolds, 1995), and as rates of ATP synthesis wane, electrogenic transport of Ca^{2+} across the plasma membrane becomes increasingly difficult, ultimately leading to cell death (Attwell & Laughlin, 2001). Therefore, excessive activation of NMDARs and the subsequent Ca^{2+} influx represents a critical step in the loss of neuronal homeostasis during hypoxia and ischemia.

Unlike humans and laboratory rodents, some animals experience variable oxygen tensions in their natural environments and have evolved a broad range of strategies to survive brain hypoxia (Larson et al., 2014). In many cases, survival during hypoxia involves entry into a hypometabolic state associated with arrested synaptic transmission and network output to conserve energy (Buck & Pamenter, 2018). However, the brain of some animals must remain active during hypoxia (Czech-Damal et al., 2014; Larson et al., 2014; Larson & Park, 2009) which presents the unique challenge of maintaining costly circuit function while avoiding hyperexcitability and excitotoxicity. An extreme example of this problem is embodied by the brainstem respiratory motor network of the American bullfrog (*Lithobates catesbeianus*). This network generates its output through mechanisms that involve excitation from AMPA and NMDA glutamate receptors (Kottick et al., 2013) and, therefore, requires ongoing aerobic metabolism to function (Adams et al., 2021). However, for several months each year, frogs overwinter in ice-covered ponds without breathing air, and blood oxygen falls to ~1-5 mmHg (Tattersall & Ultsch, 2008). This environment does not pose an immediate threat due to reduced metabolic rate in the cold (Shannon & Kramer, 1988; Tattersall & Boutilier, 1997), but during emergence at warm temperatures, the network must generate a respiratory rhythm in the background of severe hypoxia to restart breathing. To overcome this challenge, hibernation transforms the network to

function for several hours without oxygen and glucose using only internal glycogen stores and glycolysis (Bueschke, Amaral-Silva, et al., 2021). Therefore, unlike most other hypoxia-tolerant species, the adult bullfrog provides insight into plasticity that shifts a typically “hypoxia-intolerant” circuit into a state of functional hypoxia tolerance.

Hypoxia rapidly leads to hyperexcitability in the respiratory network (Adams et al., 2021; Bueschke, Amaral-Silva, et al., 2021); however, the mechanisms that constrain excitability to allow function during hypoxia upon emergence from hibernation are unclear. NMDA receptors are important for maintaining respiratory motor output (Bueschke, Amaral-Silva, et al., 2021), but they pose a threat to maintaining excitability during hypoxia due to the cost of regulating Ca^{2+} ions and the potential for excitotoxicity. Indeed, many hypoxia-tolerant vertebrates have reduced NMDAR expression or suppressed NMDAR activity in low-oxygen environments (Bickler et al., 2000; Bickler & Buck, 2007; Wilkie et al., 2008). Therefore, we hypothesized that the shift from “hypoxia intolerance” to “functional hypoxia tolerance” involves a downregulation of NMDARs within the motor network. To test this hypothesis, we assessed changes in the NMDAR tone of the respiratory motor output, and functional properties of NMDAR in motoneurons using whole-cell voltage clamp. In contrast to most of the champion hypoxia tolerant vertebrates, we demonstrate that functional hypoxia tolerance after hibernation does not involve a reduction in NMDARs, and NMDARs do not arrest during hypoxia. Instead, we find hibernation induces a large reduction in Ca^{2+}-permeability and enhances desensitization of NMDARs. These results point to plasticity that upholds the contribution of NMDARs to network output, but conserves energy and constrains excitability during hypoxia through modification of receptor function.

Results

To determine changes in overall NMDAR receptor function in the respiratory motor network between control and cold-acclimated bullfrogs, we recorded changes in NMDA receptor tone in brainstem-spinal cord preparations following exposure to the NMDAR antagonist, D-AP5 (50 μM) (Figure 7A). D-AP5 is highly selective for glutamatergic NMDARs (Morris, 1989); therefore, it represents a tool that allows us to determine the contribution of NMDARs within the respiratory motor network. If NMDAR activity were reduced or lost following cold-acclimation, we would expect a loss or reduction of NMDAR block sensitivity relative to controls. Despite our initial hypothesis, sensitivity to AP5 did not change in CA preparations ($P = 0.44$, Figure 7B). Our results suggest that overall NMDAR contribution to network function is unaltered following cold-acclimation.

Although the whole network did not change sensitivity to the block of NMDAR, we next tested if CA influences NMDAR function directly using whole-cell patch clamp. For this, we compared NMDAR current amplitude and decay kinetics to focal application of NMDAR co-agonists (NMDA, 1 mM; glycine, 10 μM) on individual vagal (respiratory) motoneurons (Figure 8A-C). Consistent with whole network responses, we saw no change in the amplitude of evoked current ($P = 0.1461$, Figure 8B) and the decay time constant between warm and cold-acclimated neurons ($P = 0.6556$, Figure 8C). These results suggest that CA does not alter excitability in vagal motoneurons by altering the functional expression of NMDARs. However, work in other hypoxia-tolerant species indicates that hypoxia may directly reduce the NMDA current amplitude (Bickler et al., 2000; Wilkie et al., 2008). Thus, we tested if hypoxia suppresses NMDAR function and found that hypoxia may suppress NMDA function to a greater extent after CA. WA neurons exhibited no change in either amplitude ($P = 0.2193$) or decay time constant ($P = 0.1189$) when exposed to hypoxia (Figure 8D). CA neurons also had no hypoxia-sensitive change in NMDARs during single pulses (Amplitude, $P = 0.8285$; Decay, $P = 0.8892$;

Figure 8E). Therefore, neither the current produced by the NMDAR nor the sensitivity to hypoxia appears to be consistent with any kind of energy-saving mechanism.

Figure 7. Cold-acclimation does not alter the NMDAR tone of respiratory motor output. (A) Representative respiritory motor bursts within stable amplitude periods in control aCSF and glutamatergic NMDAR block with D-AP5 between WA (top) and CA (bottom) preparations. Decrease in tone is correlated with NMDAR function present in the respiritory motor network. (B) Box and whisker plot comparing burst amplitude in D-AP5 relative to control between WA (left, green, n = 8) and CA (right, blue, n = 8) brainstems showing no significant change in D-AP5 sensitivity (unpaired t-test, p = 0.44). Dots represent each data point of individual experiments, and the values are mean with error bars displaying SD.

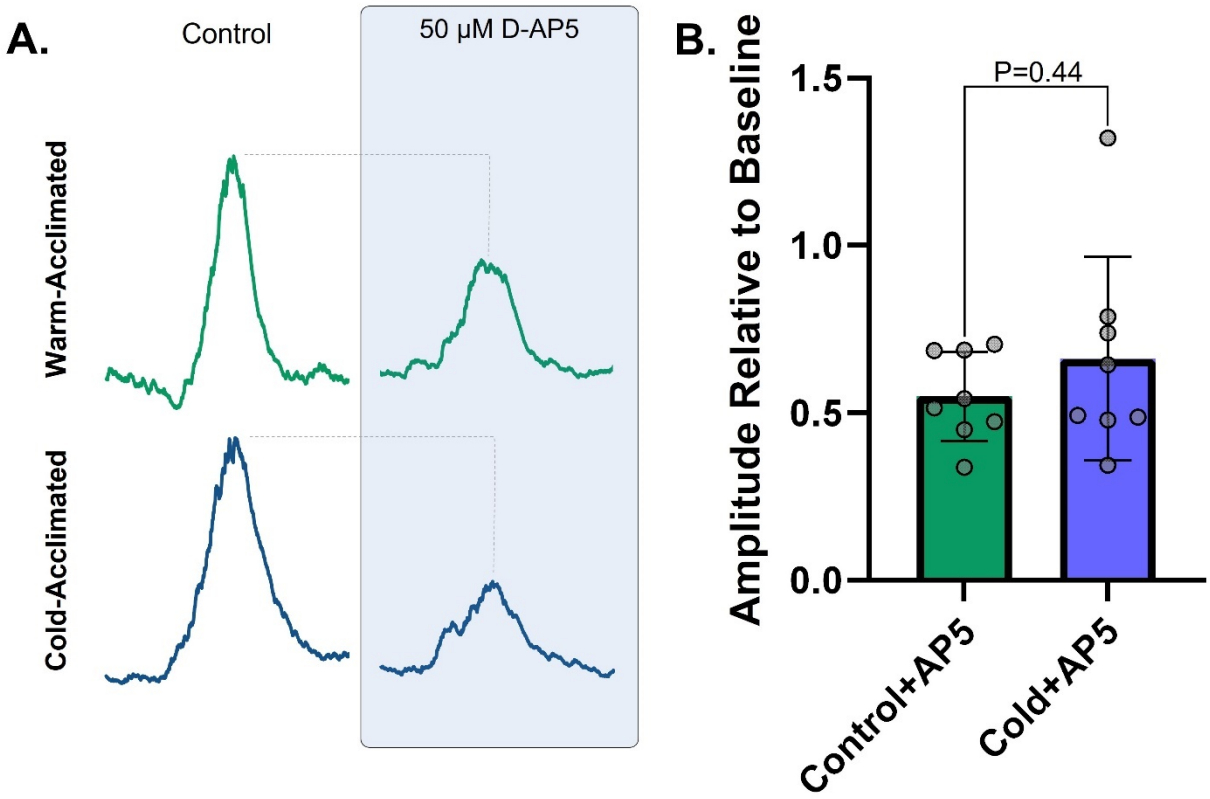

The previous results indicate that current flow through activated NMDARs is not changed after hibernation. NMDARs form tetrameric structures with GluN subunits, where eight different isoforms exist (Paoletti et al., 2013). This allows for a high diversity of NMDARs that vary in function including ion selectivity and other dynamic properties (Beesley et al., 2020). Although we did not observe changes in the overall NMDA receptor tone within the network or differences in current amplitude, we assessed the potential for changes in functional properties that may give rise to energy savings. To test for potential changes in NMDAR functional

properties, we first measured relative Ca^{2+} permeability through NMDARs in vagal motoneurons using a Ca^{2+} ion-replacement protocol in whole-cell voltage clamp and determined the NMDAR reversal potential (E_{rev}) in low and high Ca^{+2} (Figure 9). Since NMDARs are calcium-permeable, exposure to high Ca^{2+} results in depolarization of $E_{rev.}$ As expected, NMDAR currents from WA animals had a classic depolarizing shift in E_{rev} during high Ca^{2+} (12.6 mV average). Interestingly, despite overall similar current amplitude and kinetics, CA produced vagal motoneurons exhibited no significant change in E_{rev} between low and high concentrations of Ca^{2+}, demonstrating that overwintering alters NMDAR function such that Ca^{2+} permeability is reduced relative to control (Figure 9B).

Figure 8. Single-cell NMDAR activation amplitude and decay. (A) Traces showing typical responses to NMDA and glycine puff at the same scale. (B-C) NMDAR amplitude and decay is unaltered upon activation between WA and CA neurons following unpaired t tests. (D-E) Individual NMDAR amplitude and decay values before and after hypoxia. Paired t test results suggests hypoxia onset does not change neither NMDAR factor in both WA and CA neurons. Boxes show interquartile range and whiskers represent min and max values with dots showing individual data points. All data was analyzed using 1 mM Ca^{2+} in extracellular solution.

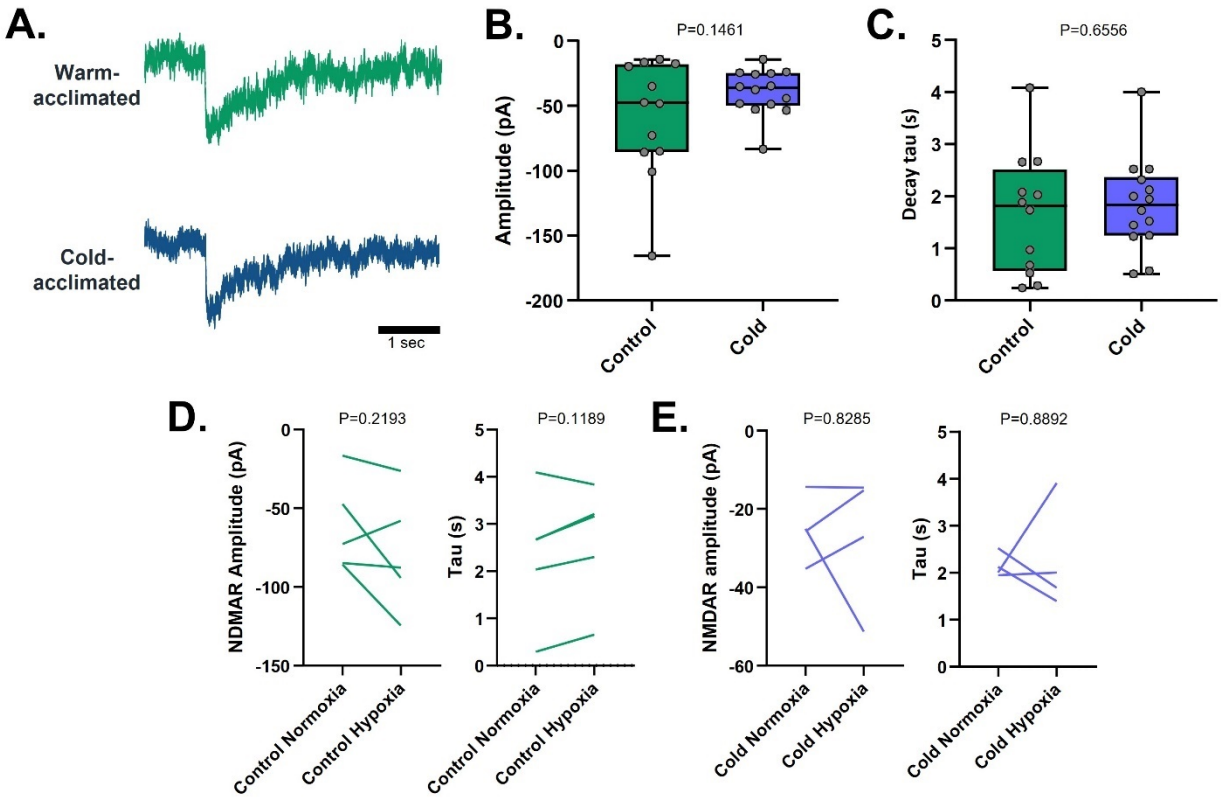

Ca^{2+} permeability is one channel characteristic; however, glutamate receptors can reduce excitability through dynamic changes in open probability. Indeed, during repetitive or continuous stimulation NMDARs decrease their open probability through a process termed "desensitization". Therefore, we tested if NMDARs in overwintered motoneurons alter their desensitization properties relative to controls. To study desensitization, 10 puffs (5-10 ms) of NMDA + glycine puffs were delivered at 0.5 Hz for 20 seconds. This protocol resulted in desensitization of NMDAR currents in WA neurons (Figure 10). As seen in Figure 10, the last current in the train was ~63% of the baseline current. Interestingly, CA neurons underwent a larger degree of desensitization, whereby the final current in the train fell by to ~36% of the control. (Figure 10A-C).

Figure 9. CA results in decreased CA^{2+} permeability in NMDARs in vagal motoneurons. (A) Whole-cell voltage clamp traces held at a range of voltages (-20 to +40 mV, Δ5 mV) responding to NMDAR activation *via* Picospritzer II puff of NMDAR agonists. Reversal potentials are highlighted to visualize the typical reduced E_{rev} right shift that CA vagal motoneurons (bottom) exhibit between low and high Ca^{2+} (1 mM and 10 mM, respectively) compared to WA controls (top). (B) Results of NMDAR E_{rev} (n = 16, all groups) show significance in 2-way ANOVA interaction (p = 0.0072), suggesting that CA effects the response to Ca^{2+}. Dots represent each data point of individual cells in each group, with boxes representing interquartile range and whiskers displaying min and max E_{rev} values.

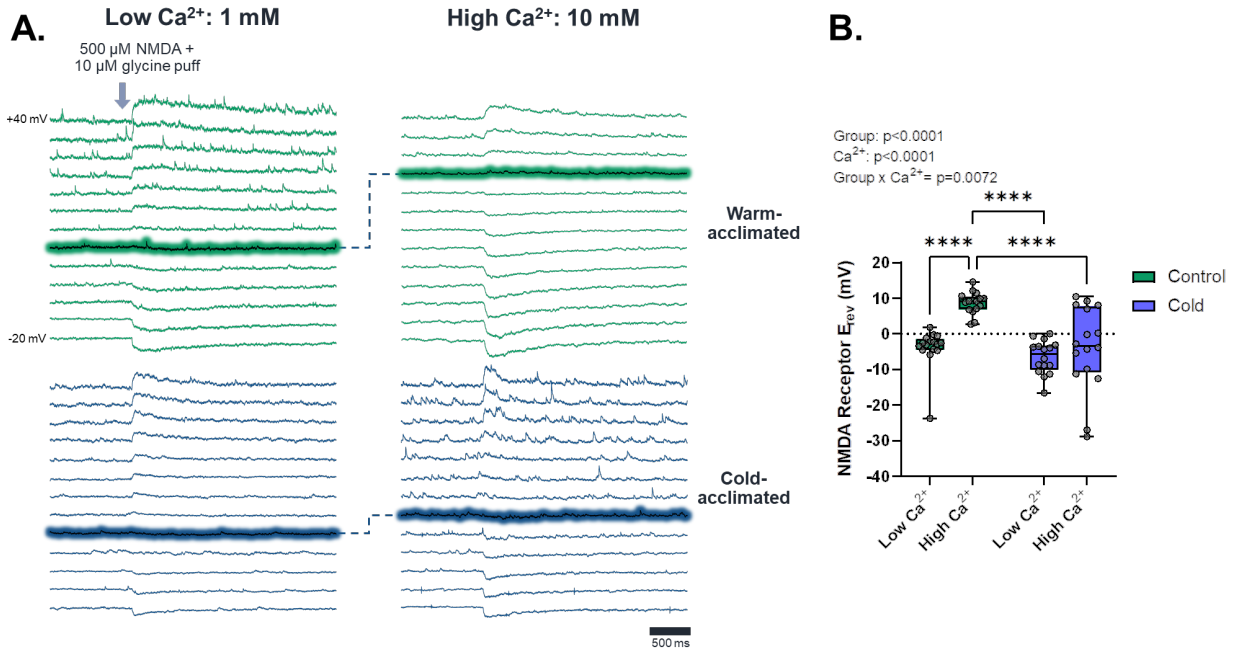

The previous results indicate that the overall NMDAR tone remains unchanged following overwintering (Figure 7); however, the functional properties are modified, consistent with enhanced energy savings (reduce P_{Ca}) and reduced excitability (greater desensitization). Thus, we hypothesized that the "normal" NMDAR characteristics of control animals typically lead to hyperexcitability during hypoxia, which would be mitigated by blocking NMDARs or reducing the permeability to Ca^{2+}/enhancing desensitization after winter. To address the first possibility, we exposed WA brainstem preparations to hypoxia, as well as WA preparations where we blocked NMDARs with D-AP5. During hypoxia, activity typically becomes chaotic followed by the loss of patterned network output (Fig 11, top trace). In the presence of NMDAR blockade, the most prominent effect we observed was that the network output becomes chaotic less frequently before failure. These results indicate that NMDARs contribute to the loss of homeostasis that leads to pathological network output during hypoxia. Next, we addressed the possibility that reducing Pc_a/enhancing desensitization may play a neuroprotective role during hypoxia upon emergence from hibernation. Our expectation was that if reducing P_{ca}/enhancing desensitization (despite the same overall NMDA tone as controls), hyperexcitable output would be less prevalent during hypoxia. Indeed, cold-acclimated preparations did not produce chaotic output normally observed during severe hypoxia in controls, and networks functioned normally for at least 1 hour. These results indicate that, despite having the same total NMDAR tone as controls, cold-acclimated networks do not produce pathological output during hypoxia. Therefore, modifications to the NMDAR properties shift the network into a protected state that can constrain excitability during severe hypoxia while maintaining the critical contribution of NMDARs to network output.

Discussion

Excitotoxicity is a major contributor to circuit dysfunction and neuronal cell death in energetic crisis, where ion dysregulation results in massive glutamatergic release (Ferdinand & Roffe, 2016). Excitatory NMDARs have a notably high permeability to Ca^{2+} ions, where Ca^{2+} plays a role in this pathological phenomenon by triggering pro-death signaling cascades (Szydlowska & Tymianski, 2010), as well as being highly energetically costly for energetic transport out of the cell. Our results reveal that the bullfrog decreases Ca^{2+} permeability in NMDARs without altering overall function. We suspect that these changes are implemented in overwintered frogs to keep neurons within the circuit stable in hypoxia by decreasing likelihood of Ca^{2+}-induced excitotoxicity. In addition to a decrease in Ca^{2+} permeability, we also discovered that NMDARs in vagal motoneurons exhibited a notable increase in desensitization following cold-acclimation. Desensitization is likely acting in this network as a method to decrease excitability specifically in the event of rapid glutamatergic signaling, which process occurs to feed the positive feedback loop of hypoxic excitotoxicity in energy crisis (Ferdinand & Roffe, 2016). Since CA brainstem-spinal cord recordings of the intact rhythmic network are completely devoid of hypoxia-induced excitable motor output, this decreased probability of this hypoxic characteristic upon blocking NMDARs in the hypoxia-intolerant network suggests that NMDARs are being altered to decrease hyperexcitable features. Taken together, observed decreases in Ca^{2+} permeability and reduced continuous excitability in NMDARs may serve to induce neuroprotection in CA motoneurons by preventing pro-death signaling cascades and ion dysregulation.

Calculating the absolute permeability of Ca^{2+} through ionotropic NMDARs that are non-selective between Ca^{2+} and Na^{+} ions provides a challenge in isolating Ca^{2+} flux. Using a derivation of the Goldman-Hodgkin-Katz equation is commonly used to calculate Ca^{2+} permeability relative to other ions (permeability ratio, P_{Ca}/P_{Na}) from comparing channel E_{rev} in Ca^{2+} ion-replacement protocols (Jatzke et al., 2002; Lewis, 1979; Wollmuth & Sakmann, 1998).

However, we had limitations with calculating permeability ratios in NMDARs due to issues in acquiring viable recordings on neurons devoid of extracellular Ca^{2+}. We therefore relied on population data, using ΔE_{rev} between Ca^{2+} concentrations to compare relative permeabilities. Since our results displayed a highly significant interaction between Ca^{2+} concentration and animal group (two-way ANOVA, P=0.0072), calculating P_{Ca}/P_{Na} outright was not necessary for these experiments.

Figure 10. NMDARs become more susceptible to desensitization following CA. (A) Representative traces of vagal motoneuron response to desensitization pulses with NMDAR agonists puffed onto the soma at 0.5 Hz. CA traces (bottom, blue) tended to have visually noticeable decreases in inward current amplitudes than WA neurons (top, green). (B) Final (10^{th}) pulse current amplitude relative to initial pulse. CA motoneurons (n = 14) had a significantly lower final amplitude than WA controls (n = 12), suggesting that CA NMDARs are more susceptible to desensitization (p = 0.0071). Dots represent each data point from individual cells, boxes represent interquartile range, and lines displaying mean with min and max values. (C) Interquartile range, mean, and min/max values for each individual pulse between WA (green) and CA (blue) motoneurons from the same data set as B.

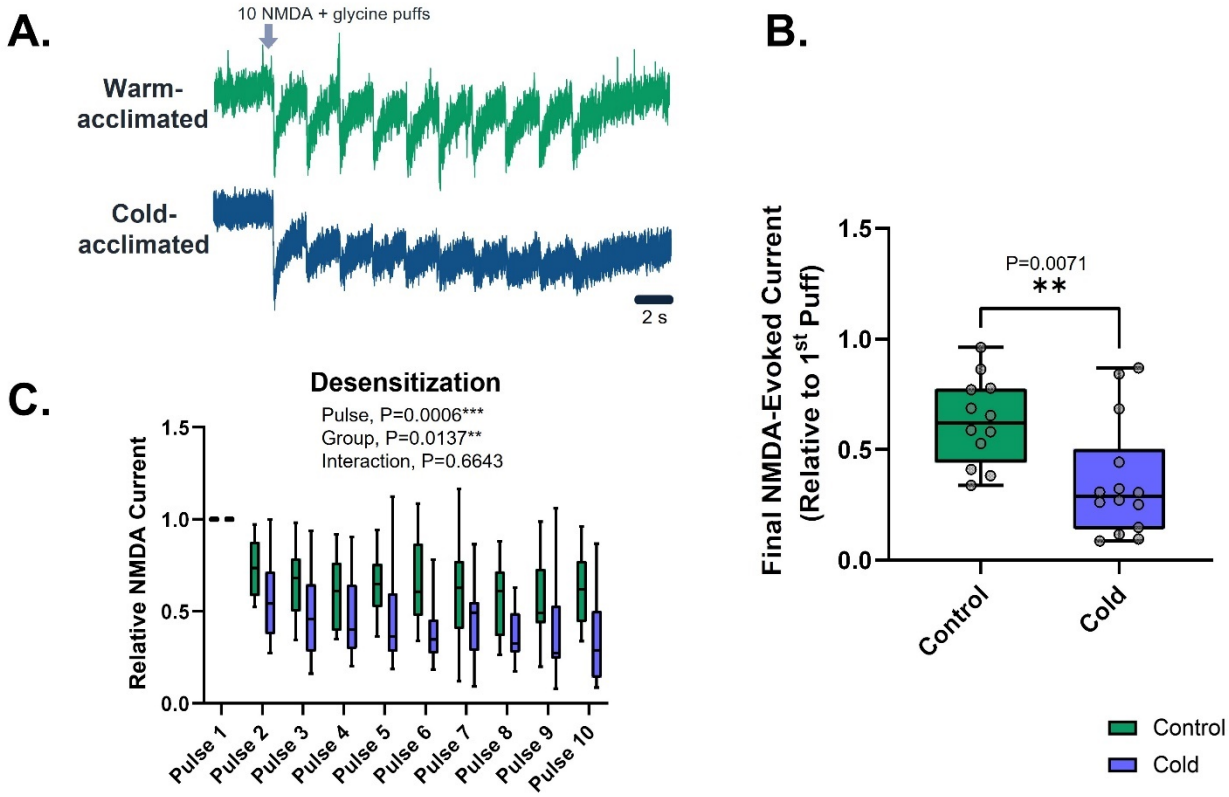

Hypoxia-tolerant species yield various mechanisms of glutamatergic suppression targeting NMDARs to prevent neuronal death (Larson et al., 2014). Species such as freshwater turtles, goldfish, and arctic ground squirrels implement silenced NMDAR activity for neuroprotection (Bickler et al., 2000; Wilkie et al., 2008; Zhao et al., 2006). Despite this common occurrence, bullfrogs do not utilize NMDAR silencing for hypoxia tolerance as demonstrated within the functioning network (Figure 7) and in individual neurons (Figure 8). NMDAR subunits are highly diverse with varying characteristics (Paoletti et al., 2013). Species such as the naked mole-rat have neurons that express higher levels of an NMDAR subtype containing GluN2D subunits that are less Ca^{2+}-permeable than other subtypes (Peterson et al., 2012). Because our results show that NMDARs are being changed by functional properties, and not through reduced function, it is worth considering what modifications can alter NMDAR function. In addition to decreased permeability being observed in naked mole-rat GluN2D NMDARs, other subtypes such as tri-heteromeric NMDARs containing a GluN3 subunit have also been proposed to show ion selectivity, where it favors Ca^{2+} permeability to Na^{+} (Beesley et al., 2020). NMDARs can also vary desensitization by GluN2 subunits are present (Dravid et al., 2008; Zhang et al., 2008). Post-translational modifications can also alter function of NMDARs such as cAMP-protein kinase A signaling cascades that can increase Ca^{2+}-permeability (Skeberdis et al., 2006). Overall, a glutamatergic circuit, such as this one requires additional adjustments in energetic efficiency to properly function primarily from anaerobic glycolysis. These findings link this necessity to altered NMDAR function that may help to decrease excitotoxicity and overall energy expenditure.

Our findings show that by modifying NMDARs, our model decreases neuronal dysfunction in hypoxia. However, these glutamate receptors are also responsible for invoking highly-important modes of homeostatic plasticity, namely long-term potentiation and depression (Sobczyk & Svoboda, 2007). Overall NMDAR suppression and changes in kinetics are potentially not being altered in this network to maximize the functional role that NMDARs play

while still preventing excitotoxic outcomes. This still has implications, however. Given that LTP and LTD are reliant on Ca^{2+} influx, this strategy for neuroprotection would not be sufficient for the long term. Our methods of NMDAR activation likely only limited us to observe NMDARs within the soma. NMDARs have known functional differences and subunit composition between synaptic and extrasynaptic locations (Paoletti et al., 2013; Papouin & Oliet, 2014). Differences in NMDAR localization can alter cellular response to Ca^{2+} influx such that synaptic NMDARs induce pro-survival responses upon activation, while extrasynaptic NMDARs induce the opposite (Lai et al., 2011). Because of this, our results only show that extrasynaptic NMDARs are being altered located at the soma. Experiments in the future should test if synaptic NMDARs retain Ca^{2+} permeability to preserve LTP and LTD.

Figure 11. NMDAR block reduces probability of hyperexcitable motor output. Fictive motor output recordings in WA control preparations have a high probability of exhibiting activity synonymous to hyperexcitable motor output with a rise in tonic activity persisting for ~1-2 minutes in hypoxia prior to energetic failure (n = 11, top trace, top pie-chart). Due to blocking NMDAR function in WA brainstems decreasing this probability (n = 8, middle trace, bottom pie chart) and hypoxia-tolerant CA brainstems being entirely absent of tonic hyperexcitability (n = 8, bottom trace) suggests that changes in NMDAR function possibly decreases excitability following overwintering.

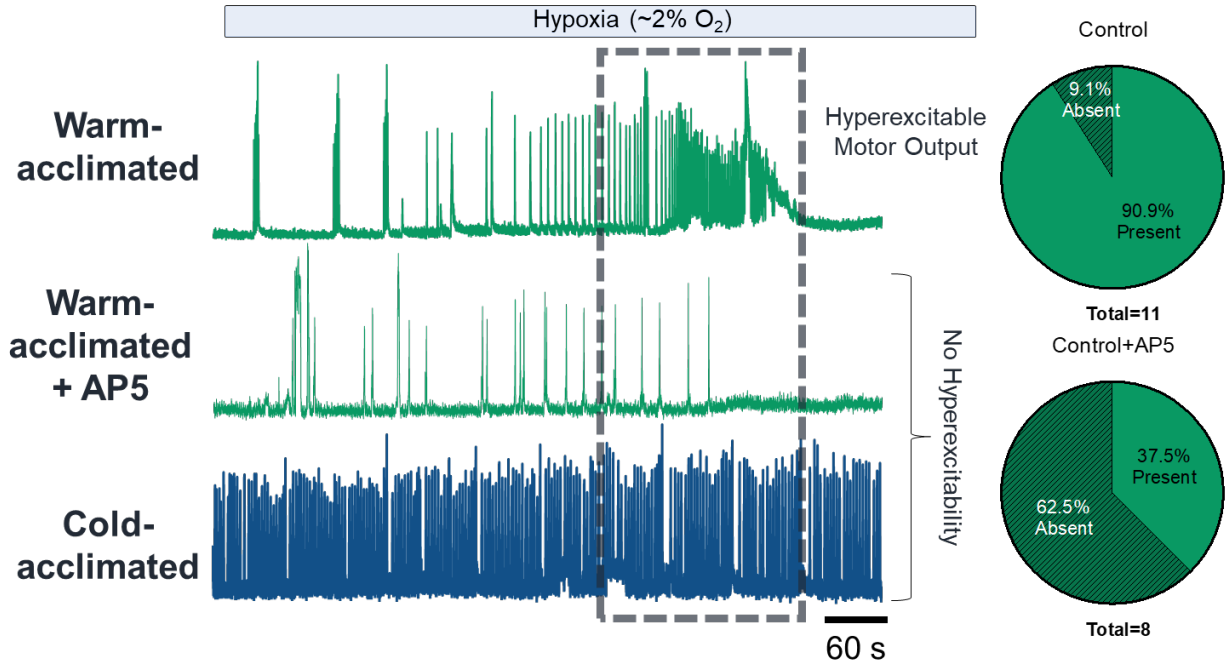

CHAPTER VI: CONCLUSIONS AND FUTURE DIRECTIONS

Circuit function requires disproportionally-large amounts of energy compared to other physiological functions within the body, making neurons incredibly susceptible to energetic failure in hypoxic conditions. The goal of this thesis research was to observe physiological characteristics of neuronal energetics in the respiratory motor network of the American bullfrog as it recently has been discovered to yield hypoxia-tolerant capabilities. This model is unique in that amphibians are not generally known to be hypoxia tolerant. Furthermore, they possess the ability to shift between being entirely intolerant to severe energetic stress, towards a state that shows a nearly 30-fold functional improvement in hypoxia following aquatic overwintering. This ability of "switching" tolerance has yet to be demonstrated in any other tolerant species.

Within this research, I uncovered: (1) Metabolic plasticity shifts circuit function to be primarily fueled *via* anaerobic mechanisms, where glucose can be supplied primarily through glycogenolysis in ischemic conditions and, (2) CA modifies glutamatergic NMDAR function to reduce Ca^{2+}-induced excitotoxicity and neuronal excitability, aiding in cell survival as well as reducing unnecessary energy consumption.

Findings from Aim 1 utilized means of pharmacological blockers of metabolism to isolate primary suppliers of energy in the CA brainstem-spinal cord preparation during severe hypoxia and OGD. Because our severe hypoxia protocol exposed the brainstem-spinal cord preparation to low levels of O_2 (~2% O_2), mitochondria may increase efficiency for electron transport to occur with reduced O_2 concentrations. However, blocking mitochondrial activity resulted in sustained activity in CA preparations, which confirmed no aerobic mechanisms occur in hypoxia (Figure 5D). In addition to the lack of aerobic mechanisms occurring, energetic failure resulting from glycolytic inhibition in CA preps suggest that this hypoxia-tolerant network operates primarily on anaerobic glycolysis. By targeting potential means of endogenous glucose supply,

we isolated localized glycogenolysis as the primary energetic fuel source in OGD within the network.

The CA brainstem shifting to anaerobic mechanisms theoretically results in a notable decrease in ATP yield, and therefore drove our interest to study mechanisms that may increase functional efficiency within the respiratory motor network. Findings from Aim II suggest that excitatory glutamatergic NMDARs in CA vagal motoneurons exhibit functional characteristics that drive an increase in energetic efficiency and neuroprotection. NMDAR Ca^{2+} conductance is minimized after overwintering, potentially to prevent pro-death signaling cascades during hyperexcitability that commonly occurs during energetic stress. We also demonstrated that NMDARs in CA neurons have increased desensitization, which limits overall conductance and therefore decreases neuronal excitability. Blocking NMDAR activity in WA brainstem-spinal cord preparations failed to improve functional duration. We have reason to speculate that this is due to other modes of energetic supply and expenditure not being optimized in WA brains. Despite this, we discovered a decreased probability of hyperexcitable motor output in WA brainstems with silenced NMDAR function, a characteristic that is also observed in CA preparations. These results suggest that decreased excitability and Ca^{2+} permeability in CA vagal motoneurons might contribute to ensuring circuit function and rigidity during severe hypoxia.

To follow up our energetic supply results, I aim to determine the role that glial cells serve in metabolism after aquatic overwintering since astrocytes are believed to contribute to energy supply for neurons *via* lactate shuttling (Magistretti et al., 1993), and are also shown to have higher levels of glycogen in overwintering bullfrogs (McDougal et al., 1968). These results directly imply an astrocyte to neuron glucose shuttle, and future experiments will directly test this idea. Although our results on NMDAR function show interesting results, the experimental design limited us to activate NMDARs that are localized on the soma. Because NMDAR localization is considered largely variable in subunit composition and function (Papouin & Oliet, 2014), as well as response to Ca^{2+} influx (Wu & Tymianski, 2018), I intend on utilizing new

techniques produced in our lab that allow for single-cell recordings within an intact network to test if synaptic NMDARs exhibit results consistent with these findings (Amaral-Silva & Santin, 2022). Furthermore, I aim to determine which modifications are responsible for altering post-hibernation NMDAR response (*i.e.* tetrameric subunit structure, post-translational modification, oxygen-sensing, *etc*.).

REFERENCES

Adams, S., Zubov, T., Bueschke, N., & Santin, J. M. (2021). Neuromodulation or energy failure? Metabolic limitations silence network output in the hypoxic amphibian brainstem. *American Journal of Physiology-Regulatory, Integrative and Comparative Physiology*, *320*(2), R105–R116. https://doi.org/10.1152/ajpregu.00209.2020

Allen, N. J., Káradóttir, R., & Attwell, D. (2005). A Preferential Role for Glycolysis in Preventing the Anoxic Depolarization of Rat Hippocampal Area CA1 Pyramidal Cells. *Journal of Neuroscience*, *25*(4), 848–859. https://doi.org/10.1523/JNEUROSCI.4157-04.2005

Amaral-Silva, L. do, & Santin, J. M. (2022). A brainstem preparation allowing simultaneous access to respiratory motor output and cellular properties of motoneurons in American bullfrogs. *Journal of Experimental Biology*, *225*(12), jeb244079. https://doi.org/10.1242/jeb.244079

Attwell, D., & Laughlin, S. B. (2001). An Energy Budget for Signaling in the Grey Matter of the Brain. *Journal of Cerebral Blood Flow & Metabolism*, *21*(10), 1133–1145. https://doi.org/10.1097/00004647-200110000-00001

Beesley, S., Sullenberger, T., & Kumar, S. S. (2020). The GluN3 subunit regulates ion selectivity within native N-methyl-d-aspartate receptors. *IBRO Reports*, *9*, 147–156. https://doi.org/10.1016/j.ibror.2020.07.009

Bickler, P. E., & Buck, L. T. (2007). Hypoxia Tolerance in Reptiles, Amphibians, and Fishes: Life with Variable Oxygen Availability. *Annual Review of Physiology*, *69*(1), 145–170. https://doi.org/10.1146/annurev.physiol.69.031905.162529

Bickler, P. E., Donohoe, P. H., & Buck, L. T. (2000). Hypoxia-Induced Silencing of NMDA Receptors in Turtle Neurons. *The Journal of Neuroscience*, *20*(10), 3522–3528. https://doi.org/10.1523/JNEUROSCI.20-10-03522.2000

Bordone, M. P., Salman, M. M., Titus, H. E., Amini, E., Andersen, J. V., Chakraborti, B., Diuba, A. V., Dubouskaya, T. G., Ehrke, E., Espindola de Freitas, A., Braga de Freitas, G., Gonçalves, R. A., Gupta, D., Gupta, R., Ha, S. R., Hemming, I. A., Jaggar, M., Jakobsen, E., Kumari, P., … Seidenbecher, C. I. (2019). The energetic brain – A review from students to students. *Journal of Neurochemistry*, *151*(2), 139–165. https://doi.org/10.1111/jnc.14829

Buck, L. T., & Pamenter, M. E. (2018). The hypoxia-tolerant vertebrate brain: Arresting synaptic activity. *Comparative Biochemistry and Physiology Part B: Biochemistry and Molecular Biology*, *224*, 61–70. https://doi.org/10.1016/j.cbpb.2017.11.015

Bueschke, N., Amaral-Silva, L. do, Adams, S., & Santin, J. M. (2021). Transforming a neural circuit to function without oxygen and glucose delivery. *Current Biology*, *31*(24), R1564–R1565. https://doi.org/10.1016/j.cub.2021.11.003

Bueschke, N., Amaral-Silva, L., Hu, M., & Santin, J. M. (2021). Lactate ions induce synaptic plasticity to enhance output from the central respiratory network. *The Journal of Physiology*, *599*(24), 5485–5504. https://doi.org/10.1113/JP282062

Cheng, X., Vinokurov, A. Y., Zherebtsov, E. A., Stelmashchuk, O. A., Angelova, P. R., Esteras, N., & Abramov, A. Y. (2021). Variability of mitochondrial energy balance across brain regions. *Journal of Neurochemistry*, *157*(4), 1234–1243. https://doi.org/10.1111/jnc.15239

Czech-Damal, N. U., Geiseler, S. J., Hoff, M. L. M., Schliep, R., Ramirez, J.-M., Folkow, L. P., & Burmester, T. (2014). The role of glycogen, glucose and lactate in neuronal activity during hypoxia in the hooded seal (Cystophora cristata) brain. *Neuroscience*, *275*, 374–383. https://doi.org/10.1016/j.neuroscience.2014.06.024

Dravid, S. M., Prakash, A., & Traynelis, S. F. (2008). Activation of recombinant NR1/NR2C NMDA receptors: NR1/NR2C receptor activation. *The Journal of Physiology*, *586*(18), 4425–4439. https://doi.org/10.1113/jphysiol.2008.158634

Ferdinand, P., & Roffe, C. (2016). Hypoxia after stroke: A review of experimental and clinical evidence. *Experimental & Translational Stroke Medicine*, *8*(1), 9. https://doi.org/10.1186/s13231-016-0023-0

Fournier, S., Allard, M., Roussin, S., & Kinkead, R. (2007). Developmental changes in central O2 chemoreflex in *Rana catesbeiana*: The role of noradrenergic modulation. *Journal of Experimental Biology*, *210*(17), 3015–3026. https://doi.org/10.1242/jeb.005983

Fournier, S., & Kinkead, R. (2008). Role of pontine neurons in central O2 chemoreflex during development in bullfrogs (Lithobates catesbeiana). *Neuroscience*, *155*(3), 983–996. https://doi.org/10.1016/j.neuroscience.2008.05.044

Frerichs, K. U., Kennedy, C., Sokoloff, L., & Hallenbeck, J. M. (1994). Local Cerebral Blood Flow during Hibernation, a Model of Natural Tolerance to "Cerebral Ischemia." *Journal of Cerebral Blood Flow & Metabolism*, *14*(2), 193–205. https://doi.org/10.1038/jcbfm.1994.26

Harris, J. J., Jolivet, R., & Attwell, D. (2012). Synaptic Energy Use and Supply. *Neuron*, *75*(5), 762–777. https://doi.org/10.1016/j.neuron.2012.08.019

Hille, B. (2001). *Ion channels of excitable membranes* (3rd ed). Sinauer.

Jatzke, C., Junryo Watanabe, & Wollmuth, L. P. (2002). Voltage and concentration dependence of Ca^{2+} permeability in recombinant glutamate receptor subtypes. *The Journal of Physiology*, *538*(1), 25–39. https://doi.org/10.1113/jphysiol.2001.012897

Kerem, D., Hammond, D. D., & Elsner, R. (1973). Tissue glycogen levels in the Weddell seal, Leptonychotes weddelli: A possible adaptation to asphyxial hypoxia. *Comparative Biochemistry and Physiology Part A: Physiology*, *45*(3), 731–736. https://doi.org/10.1016/0300-9629(73)90076-5

Kottick, A., Baghdadwala, M. I., Ferguson, E. V., & Wilson, R. J. A. (2013). Transmission of the respiratory rhythm to trigeminal and hypoglossal motor neurons in the American Bullfrog

(Lithobates catesbeiana). *Respiratory Physiology & Neurobiology*, *188*(2), 180–191. https://doi.org/10.1016/j.resp.2013.06.008

Lai, T. W., Shyu, W.-C., & Wang, Y. T. (2011). Stroke intervention pathways: NMDA receptors and beyond. *Trends in Molecular Medicine*, *17*(5), 266–275. https://doi.org/10.1016/j.molmed.2010.12.008

Larson, J., Drew, K. L., Folkow, L. P., Milton, S. L., & Park, T. J. (2014). No oxygen? No problem! Intrinsic brain tolerance to hypoxia in vertebrates. *Journal of Experimental Biology*, *217*(7), 1024–1039. https://doi.org/10.1242/jeb.085381

Larson, J., & Park, T. J. (2009). Extreme hypoxia tolerance of naked mole-rat brain. *NeuroReport*, *20*(18), 1634–1637. https://doi.org/10.1097/WNR.0b013e32833370cf

Lewis, C. A. (1979). Ion-concentration dependence of the reversal potential and the single channel conductance of ion channels at the frog neuromuscular junction. *The Journal of Physiology*, *286*, 417–445.

Li, S., Hafeez, A., Noorulla, F., Geng, X., Shao, G., Ren, C., Lu, G., Zhao, H., Ding, Y., & Ji, X. (2017). Preconditioning in neuroprotection: From hypoxia to ischemia. *Progress in Neurobiology*, *157*, 79–91. https://doi.org/10.1016/j.pneurobio.2017.01.001

Lutas, A., Birnbaumer, L., & Yellen, G. (2014). Metabolism Regulates the Spontaneous Firing of Substantia Nigra Pars Reticulata Neurons via K_{ATP} and Nonselective Cation Channels. *The Journal of Neuroscience*, *34*(49), 16336–16347. https://doi.org/10.1523/JNEUROSCI.1357-14.2014

Madison, D. V., Malenka, R. C., & Nicoll, R. A. (1991). Mechanisms Underlying Long-Term Potentiation of Synaptic Transmission. *Annual Review of Neuroscience*, *14*(1), 379–397. https://doi.org/10.1146/annurev.ne.14.030191.002115

Magistretti, P. J., Sorg, O., Yu, N., Martin, J. L., & Pellerin, L. (1993). Neurotransmitters regulate energy metabolism in astrocytes: Implications for the metabolic trafficking between

neural cells. *Developmental Neuroscience*, *15*(3–5), 306–312. https://doi.org/10.1159/000111349

McDougal, D. B., Holowach, J., Howe, M. C., Jones, E. M., & Thomas, C. A. (1968). The effects of anoxia upon energy sources and selected metabolic intermediates in the brains of fish, frog and turtle. *Journal of Neurochemistry*, *15*(7), 577–588. https://doi.org/10.1111/j.1471-4159.1968.tb08956.x

Morris, R. G. (1989). Synaptic plasticity and learning: Selective impairment of learning rats and blockade of long-term potentiation in vivo by the N-methyl-D-aspartate receptor antagonist AP5. *The Journal of Neuroscience: The Official Journal of the Society for Neuroscience*, *9*(9), 3040–3057.

Pamenter, M. E., Hogg, D. W., Ormond, J., Shin, D. S., Woodin, M. A., & Buck, L. T. (2011). Endogenous GABAA and GABAB receptor-mediated electrical suppression is critical to neuronal anoxia tolerance. *Proceedings of the National Academy of Sciences*, *108*(27), 11274–11279. https://doi.org/10.1073/pnas.1102429108

Paoletti, P., Bellone, C., & Zhou, Q. (2013). NMDA receptor subunit diversity: Impact on receptor properties, synaptic plasticity and disease. *Nature Reviews Neuroscience*, *14*(6), 383–400. https://doi.org/10.1038/nrn3504

Papouin, T., & Oliet, S. H. R. (2014). Organization, control and function of extrasynaptic NMDA receptors. *Philosophical Transactions of the Royal Society B: Biological Sciences*, *369*(1654), 20130601. https://doi.org/10.1098/rstb.2013.0601

Peterson, B. L., Park, T. J., & Larson, J. (2012). Adult naked mole-rat brain retains the NMDA receptor subunit GluN2D associated with hypoxia tolerance in neonatal mammals. *Neuroscience Letters*, *506*(2), 342–345. https://doi.org/10.1016/j.neulet.2011.11.042

Rangaraju, V., Calloway, N., & Ryan, T. A. (2014). Activity-driven local ATP synthesis is required for synaptic function. *Cell*, *156*(4), 825–835. https://doi.org/10.1016/j.cell.2013.12.042

Rossi, D. J., Brady, J. D., & Mohr, C. (2007). Astrocyte metabolism and signaling during brain ischemia. *Nature Neuroscience*, *10*(11), 1377–1386. https://doi.org/10.1038/nn2004

Samosudova, N. V., Reutov, V. P., & Larionova, N. P. (2010). Role of Glycogen in Processes of Cerebellar Glial Cells under Conditions of Its Damage with Sodium Nitrite. *Bulletin of Experimental Biology and Medicine*, *150*(2), 247–250. https://doi.org/10.1007/s10517-010-1116-8

Santin, J. M., & Hartzler, L. K. (2013). Respiratory signaling of locus coeruleus neurons during hypercapnic acidosis in the bullfrog, Lithobates catesbeianus. *Respiratory Physiology & Neurobiology*, *185*(3), 553–561. https://doi.org/10.1016/j.resp.2012.11.002

Schmidt, M. M., & Dringen, R. (2009). Differential Effects of Iodoacetamide and Iodoacetate on Glycolysis and Glutathione Metabolism of Cultured Astrocytes. *Frontiers in Neuroenergetics*, *1*, 1. https://doi.org/10.3389/neuro.14.001.2009

Shannon, P., & Kramer, D. (1988). Water depth alters respiratory behaviour of Xenopus laevis. *Journal of Experimental Biology*, *137*(1), 597–602. https://doi.org/10.1242/jeb.137.1.597

Skeberdis, V. A., Chevaleyre, V., Lau, C. G., Goldberg, J. H., Pettit, D. L., Suadicani, S. O., Lin, Y., Bennett, M. V. L., Yuste, R., Castillo, P. E., & Zukin, R. S. (2006). Protein kinase A regulates calcium permeability of NMDA receptors. *Nature Neuroscience*, *9*(4), 501–510. https://doi.org/10.1038/nn1664

Sobczyk, A., & Svoboda, K. (2007). Activity-Dependent Plasticity of the NMDA-Receptor Fractional Ca2+ Current. *Neuron*, *53*(1), 17–24. https://doi.org/10.1016/j.neuron.2006.11.016

Somjen, G. G. (2001). Mechanisms of Spreading Depression and Hypoxic Spreading Depression-Like Depolarization. *Physiological Reviews*, *81*(3), 1065–1096. https://doi.org/10.1152/physrev.2001.81.3.1065

Stafford, N., Wilson, C., Oceandy, D., Neyses, L., & Cartwright, E. J. (2017). The Plasma Membrane Calcium ATP ASES and Their Role as Major New Players in Human Disease. *Physiological Reviews*, *97*(3), 1089–1125. https://doi.org/10.1152/physrev.00028.2016

Szydlowska, K., & Tymianski, M. (2010). Calcium, ischemia and excitotoxicity. *Cell Calcium*, *47*(2), 122–129. https://doi.org/10.1016/j.ceca.2010.01.003

Tattersall, G. J., & Boutilier, R. G. (1997). Balancing hypoxia and hypothermia in cold-submerged frogs. *The Journal of Experimental Biology*, *200*(Pt 6), 1031–1038. https://doi.org/10.1242/jeb.200.6.1031

Tattersall, G. J., & Ultsch, G. R. (2008). Physiological Ecology of Aquatic Overwintering in Ranid Frogs. *Biological Reviews*, *83*(2), 119–140. https://doi.org/10.1111/j.1469-185X.2008.00035.x

Walls, A. B., Sickmann, H. M., Brown, A., Bouman, S. D., Ransom, B., Schousboe, A., & Waagepetersen, H. S. (2008). Characterization of 1,4-dideoxy-1,4-imino-d-arabinitol (DAB) as an inhibitor of brain glycogen shunt activity. *Journal of Neurochemistry*, *105*(4), 1462–1470. https://doi.org/10.1111/j.1471-4159.2008.05250.x

White, R. J., & Reynolds, I. J. (1995). Mitochondria and Na+/Ca2+ exchange buffer glutamate-induced calcium loads in cultured cortical neurons. *The Journal of Neuroscience: The Official Journal of the Society for Neuroscience*, *15*(2), 1318–1328.

Wilkie, M. P., Pamenter, M. E., Alkabie, S., Carapic, D., Shin, D. S. H., & Buck, L. T. (2008). Evidence of anoxia-induced channel arrest in the brain of the goldfish (Carassius auratus). *Comparative Biochemistry and Physiology Part C: Toxicology & Pharmacology*, *148*(4), 355–362. https://doi.org/10.1016/j.cbpc.2008.06.004

Winmill, R. E., Chen, A. K., & Hedrick, M. S. (2005). Development of the respiratory response to hypoxia in the isolated brainstem of the bullfrog *Rana catesbeiana*. *Journal of Experimental Biology*, *208*(2), 213–222. https://doi.org/10.1242/jeb.01399

Wollmuth, L. P., & Sakmann, B. (1998). Different Mechanisms of Ca2+ Transport in NMDA and Ca2+-permeable AMPA Glutamate Receptor Channels. *The Journal of General Physiology*, *112*(5), 623–636.

Wu, Q. J., & Tymianski, M. (2018). Targeting NMDA receptors in stroke: New hope in neuroprotection. *Molecular Brain*, *11*(1), 15. https://doi.org/10.1186/s13041-018-0357-8

Zhang, W., Howe, J. R., & Popescu, G. K. (2008). Distinct gating modes determine the biphasic relaxation of NMDA receptor currents. *Nature Neuroscience*, *11*(12), 1373–1375. https://doi.org/10.1038/nn.2214

Zhao, H. W., Ross, A. P., Christian, S. L., Buchholz, J. N., & Drew, K. L. (2006). Decreased NR1 Phosphorylation and Decreased NMDAR Function in Hibernating Arctic Ground Squirrels. *Journal of Neuroscience Research*, *84*(2), 291–298. https://doi.org/10.1002/jnr.20893

APPENDIX A: COMPARING THEORETICAL COST OF ACTIVE TRANSPORT OF IONS

Gibb's Free Energy in terms of the concentration of products and reactants:

$$\Delta G = \Delta G° + RTlnQ$$

Gibb's Free Energy in terms of potential difference in charge:

$$\Delta G = -nFE$$

Nernst equation that defines equilibrium potential:

$$E_{ion} = \frac{RT}{nF}\ln\left(\frac{[ion_{out}]}{[ion_{in}]}\right)$$

Solving for the energy expended in Ca^{2+} uniport:

$$\Delta G_{pump} = \Delta G^{\circ}{}_{pump} + \Delta G_{ATP} + RTlnQ_{Ca}$$

$$-nFE^{\circ} = \Delta G_{pump} - \Delta G_{ATP} - RTlnQ_{Ca}$$

$$E^{\circ} = \frac{-\Delta G}{nF} + \frac{-\Delta G_{ATP}}{nF} + E_{Ca}$$

$$\Delta G = nF\left(-E^{\circ} + \frac{\Delta G_{ATP}}{nF} + E_{Ca}\right)$$

By approximating E_{Ca} as +120 mV, the theoretical energy yield required for Ca^{2+} uniport is approximately -26.8 kJ/mol.

Solving for energy expended in Na^{+} export via Na^{+}/K^{+} ATPase:

$$\Delta G_{pump} = \Delta G^{\circ}{}_{pump} + \Delta G_{ATP} + 3(RTlnQ_{Na}) + 2(RTlnQ_{K})$$

$E^{\circ} = \frac{-\Delta G}{nF} + \frac{\Delta G_{ATP}}{nF} + 3(E_{Na}) - 2(E_{K})$*

$\Delta G = nF\left(-E^{\circ} + \frac{\Delta G_{ATP}}{nF} + 3(E_{Na}) - 2(E_{K})\right)$

$\frac{\Delta G}{3} = Energy\ per\ Na\ ion$

*The Nernst equation does not consider reaction direction in the value of Q, therefore the reciprocal is recorded.

By approximating E_{Na} as +50 mV and E_K as -90 mV, the theoretical energy expenditure required to transport one Na^+ ion is approximately 7.5 kJ/mol.

When comparing the energy expenditure on active transport between 1 mol Ca^{2+} (-26.8 kJ/mol) and Na^+(-7.5 kJ/mol), we see that the theoretical cost to actively transport Ca^{2+} outside of a neuron using the primary and most efficient physiological method is approximately 300% more expensive than that of Na^+ active transport.